J. Fluid Mech. (1995), *vol.* 305, *pp.* 127–157

Coherent motions and heat transfer in a wall turbulent shear flow

By Y. NAGANO AND M. TAGAWA

Department of Mechanical Engineering, Nagoya Institute of Technology, Gokiso-cho, Showa-ku, Nagoya 466, Japan

(Received 3 November 1993 and in revised form 14 August 1995)

In wall turbulence, it is widely accepted that the coherent motions determine the essential features of turbulent transport phenomena. In the present study, we have refined a trajectory-based detection algorithm for coherent motions and have investigated the relationship between coherent motions and scalar (heat) transfer from a structural point of view, i.e. trajectory analysis of the VITA heat transfer events, extraction of key flow modules and the relevant heat transport, and the prediction of passive scalar transfer by means of an autoregressive (AR) model. As a result, it is shown that the phase relationship of fluctuating velocity components dominates the essential characteristics of the transport processes of heat and momentum in wall turbulence and there exist distinct differences in individual correspondence between the coherent motions and heat transport processes, neither of which can be revealed by the widely used VITA technique. Also, the AR model is shown to provide good time-series predictions for turbulent heat transfer associated with coherent structures near the wall.

1. Introduction

In wall turbulence, ejections and sweeps are the primary constitutive motions of coherent structures. As surveyed extensively by Robinson (1991*a*, *b*), it has been established that these coherent motions play an important role in maintaining the turbulence production mechanism and determine most of the essential features of turbulent transport phenomena near the wall. Thus, there would seem to be no question that the fundamental aspects of scalar (heat) transfer in wall turbulence may be characterized by the coherent motions. In earlier papers, Nagano & Tagawa (1988, 1990) showed that the near-wall turbulent structures almost always control the statistical characteristics of turbulent transport of a passive scalar. However, further detailed and concrete knowledge of the coherent structures and relevant turbulent heat transfer is needed in connection with flow and heat transfer control. To investigate the details of the coherent structures and to evaluate their role in turbulent heat transfer quantitatively, we need an appropriate methodology for detecting and extracting coherent motions from seemingly random time-series data of turbulence. Current representative detection schemes for coherent motions are the variable-interval time average (VITA) method (Blackwelder & Kaplan 1976), the quadrant splitting technique (Lu & Willmarth 1973) and many modifications thereof (e.g. see Bogard & Tiederman 1986). However, it is extremely difficult to rank these detection methods since each method has both advantages and disadvantages. In addition, we still have little idea of what features of the coherent motions can be obtained

by each detection scheme. In this respect, Spina, Donovan & Smits (1991) have recently discussed the importance of identifying the relationship between the VITA and quadrant techniques (Alfredsson & Johansson 1984) in terms of similarities and differences in the 'coherent structures' extracted.

As mentioned above, the heat transfer associated with coherent structures in wall turbulence is not yet sufficiently clear, compared with the corresponding momentum transfer. In this category, one can refer to the various investigations pertaining to the streaky structures of a thermal boundary layer (Iritani, Kasagi & Hirata 1985; Kasagi 1990), the ensemble-averaged structures of heat and momentum transfer using different detection schemes (Subramanian *et al.* 1982), structural analysis of various types of moments of velocity and temperature near the wall (Nagano & Tagawa 1988, 1990), basic near-wall flow patterns responsible for heat transfer (Nagano & Hishida 1990), and direct numerical simulations of wall turbulent heat transfer (Kim & Moin 1989; Kasagi & Ohtsubo 1993).

In the present study, we refine a trajectory analysis developed by Nagano & Hishida (1990) to improve its reliability and accuracy in coherent pattern recognition, and depict and simulate the detailed processes of heat transfer driven by the coherent motions near the wall. Emphasis is laid on: (i) analysis of the relationship between the motions detected by the VITA technique and the heat transport; (ii) reasonable extraction of key constituent patterns of the coherent motions and heat transfer; (iii) identification of typical phases of the ejections observed in a flow-visualization experiment (Bogard & Tiederman 1987) on the basis of the trajectory analysis; and (iv) prediction of the extracted basic patterns by using the autoregressive (AR) model.

In the following, terminology is based on the latest community-wide project on quasi-coherent structures in the turbulent boundary layer (Kline 1990; Robinson, Kline & Spalart 1990).

2. Experimental apparatus and procedure

The experimental apparatus employed in the present study is the same as that used in our previous studies (Hishida & Nagano 1979; Hishida, Nagano & Tagawa 1986; Nagano & Tagawa 1988). The experiment was performed in an air flow in a 45.68 mm ID reamed brass tube heated to a uniform wall temperature of 100 °C at a Reynolds number (based on bulk velocity and pipe diameter) of 40000. Measurements were performed at a location 167 diameters downstream from the pipe inlet and 40 diameters downstream from the beginning of the heated section. Both velocity and thermal fields were fully developed at this location (Hishida & Nagano 1978*a*; Nagano, Sato & Tagawa 1995). The mean characteristics of the flow are given in table 1, where $R_\theta = \overline{U}_c\theta/\nu$ ($\overline{U}_c$ being the centreline velocity) is the momentum thickness Reynolds number, $\overline{T}_w$ and $\overline{T}_c$ are the wall and centreline temperatures, q_w is the wall heat flux, u_τ is the friction velocity, and t_τ is the friction temperature defined as $t_\tau = q_w/\rho c_p u_\tau$. Since the pipe wall of the test section was heated by saturated steam, q_w was measured from the rate of condensation of the steam obtained in separated heating sections. The wall shear stress was obtained very accurately from the static pressure gradient along the pipe axis. The details of these measurements are described in Hishida & Nagano (1978*a*).

In a heated flow, fluctuations of velocity components, u (axial) and v (wall-normal) and temperature, t, were simultaneously measured with a specially devised three-wire probe (Hishida *et al.* 1986). The probe consisted of two hot-wires, one a symmetrically bent V-shaped wire (Hishida & Nagano 1988*a*, *b*; Nagano & Tsuji 1994) and the other

Re	R_θ	$\overline{U}_c$ (m s^{-1})	u_τ (m s^{-1})	$\overline{T}_w$ (°C)	$\overline{T}_c$ (°C)	t_τ (°C)	q_w (W m^{-2})
4×10^4	1032	17.2	0.79	100.3	41.2	2.9	2333

TABLE 1. Mean parameters of the velocity and thermal fields

a single straight one, together with a cold wire (Hishida & Nagano 1978*b*; Nagano & Tsuji 1994). In order to ascertain the reliability of velocity measurements in a heated flow, we have also performed X-probe measurements under an isothermal condition, in which two V-shaped hot wires with wire separation of less than 0.26 mm were used in conformity with the latest knowledge of the best design of an X-probe (Tagawa, Tsuji & Nagano 1992). The V-shaped hot wires have proven highly effective for the measurement of near-wall turbulence, where the conventional X-wire anemometry technique is subject to large errors, if it can be used at all (Nagano & Tagawa 1988; Nagano & Tsuji 1994). Note that the probe was constructed as small as practicable in order to assure spatial resolution without causing any thermal and aerodynamic interference between the wires. Namely, the sensing part was kept less than 6η (η is the Kolmogorov microscale defined by $\eta = (\nu^3/\varepsilon)^{1/4}$), where η was estimated from the dissipation rate of turbulence energy, ε, measured in the buffer region (see Nagano & Hishida 1985). In the outer region, the dissipation rate ε is much smaller than that in the near-wall region. Thus, η becomes large in the outer region and the size of the sensing part of the hot wire normalized by η is consistently much smaller than 6, i.e. spatial resolution becomes higher. For the temperature measurement of the present study, we have used a 3 μm diameter tungsten wire, whose raw cut-off frequency is about 720 Hz at a flow velocity 10 m s^{-1}. The frequency response of this resistance wire has been compensated by an electronic circuit as described in Hishida & Nagano (1978*b*). As a result, the compensated frequency response of the wire becomes about 10 kHz (this value can be obtained by giving electric step heating to the wire), which covers most of the spectral range of temperature fluctuations in this experiment. Since heat loss due to the end conduction, which occurs for a shorter cold wire, lowers the sensitivity to temperature fluctuations, appropriate corrections for this effect have been performed according to Wroblewski & Eibeck (1991) and Tsuji, Nagano & Tagawa (1992). As a result, the peak value near the wall is almost equal to that of the DNS data by Kasagi, Tomita & Kuroda (1992) (for details, see Nagano *et al.* 1995). All data were recorded in analog form with an FM data recorder (TEAC SR-31) and then reproduced for conversion to digital form.

The digitized data were stored on magnetic tape with a 12 bit analog-to-digital converter (TEAC DR-2000). For each set of u-, v- and t-fluctuations, the real-time sampling frequency was 32 kHz, and the number of data points per measurement was 52428. It was confirmed that the sampling frequency and the data length were sufficiently adequate to obtain reliable statistical values. Any slight phase lag in high-frequency temperature fluctuations that occurred in a compensation circuit was eliminated almost completely by the following method: first, the Fourier transform was performed on signals of temperature fluctuation; secondly, phase discrepancy determined by a transfer function of the circuit for the simultaneous measurement of velocity and temperature (Hishida & Nagano 1978*b*) was corrected to each Fourier coefficient; finally, the inverse Fourier transform was performed to obtain true temperature fluctuations. As a consequence, the phase lag between the temperature and velocity fluctuation measurements becomes almost negligible.

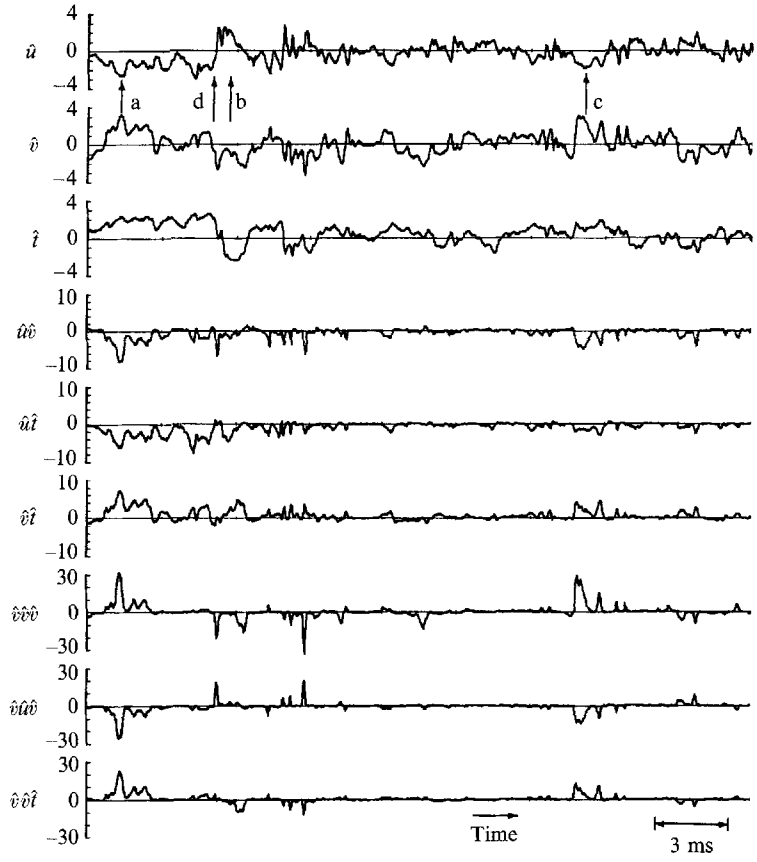

FIGURE 1. Simultaneous signal traces of turbulent quantities related to heat and momentum transfer ($y^+ = 18.5$).

Conditional sampling and averaging for these digital data were made on a FACOM M-780/20 computer system.

3. Pictorial structure examination

Typical instantaneous fluctuations of the velocity components u and v, temperature t, turbulent shear stress uv, streamwise and wall-normal turbulent heat fluxes ut and vt, and triple velocity and temperature correlations v^3, vuv and vvt, are presented in figure 1. In this figure and also in what follows, a circumflex denotes the normalization by the respective r.m.s. value as $\hat{u} = u/u_{rms}$, $\hat{v} = v/v_{rms}$ and $\hat{t} = t/t_{rms}$, where $u_{rms} = (\overline{u^2})^{1/2}$, $v_{rms} = (\overline{v^2})^{1/2}$ and $t_{rms} = (\overline{t^2})^{1/2}$. These visual data were taken at a representative position in the buffer region, i.e. $y^+(\equiv yu_\tau/\nu) = 18.5$, where very active coherent motions are usually observed (Robinson 1991*a*).

In figure 1, regions where remarkable heat and momentum transport occurs are indicated by the letters a–c. According to the quadrant splitting classification (Lu & Willmarth 1973; Nagano & Tagawa 1988), regions a and c correspond to ejections (Q2-motions) which are the outward ($v > 0$) motions of low-speed fluid with high temperature ($u < 0$, $t > 0$), and region b is an example of sweeps (Q4-motions) which are the wallward ($v < 0$) motions of high-speed fluid with low temperature ($u > 0$, $t < 0$). On the other hand, event d indicates that the interface between the ejection

and the sweep has passed the measuring probe. The u-signal pattern around d consists of a gradual deceleration followed by a strong acceleration (Blackwelder & Kaplan 1976; Wallace, Brodkey & Eckelmann 1977). This is a typical phenomenon observed frequently in wall turbulence, which can be explained by the meandering of streamwise streaky structures near the wall around which ejections and sweeps tend to occur side by side (Robinson 1991*a*; Robinson *et al.* 1990; Johansson, Alfredsson & Kim 1991). Note that it is this type of event that is usually detected by the VITA technique (Blackwelder & Kaplan 1976; Johansson & Alfredsson 1982). Thus, we use the term VITA events for particular motions detected by the VITA technique. As seen in figure 1, heat and momentum transport driven by coherent motions occurs intermittently, and thus it is easy to distinguish very active regions from inactive backgrounds. It is also clear that the turbulent transport of the Reynolds stresses and turbulent heat fluxes, i.e. triple products, is almost always synchronized with the coherent motions such as ejections and sweeps (Nagano & Tagawa 1990). Furthermore, a large amount of heat and momentum transfer is found to occur in durable low-velocity and high-temperature regions rather than the VITA-event regions such as position d in figure 1. Although it would be presumptions to conclude from this figure alone that the region a belongs to a low-speed streak, we would be generally safe in regarding a low-velocity and high-temperature region with a long duration as a low-speed streak from the established flow and thermal visualization results (Iritani *et al.* 1985). In short, an interface region between a gradual velocity deceleration and a strong acceleration, which is selectively detected by the VITA method, is not the only factor contributing to active heat and momentum transport. The details will be discussed later.

To investigate the local similarity between the thermal and velocity fields in a wall turbulent shear flow, we have applied the wavelet analysis (Farge 1992) to the instantaneous velocity and temperature fluctuations u, v and t. As discussed by Hunt *et al.* (1993), the wavelet transform can give information on both scale and position of an event simultaneously and thus is an effective tool suitable for the analysis of turbulent phenomena. The results can be summarized briefly as follows (figures not shown). The contour map (scale *vs.* time) of the wavelet-transformed u is quite similar to that of t, particularly in the large-scale regions. On the other hand, there is no such strong similarity in the large-scale regions between v and t. This is an important aspect of turbulent heat transfer, suggesting that the production mechanism of the turbulent heat flux vt is different from that of ut. As for v and t correspondence, it is found that t-fluctuations are correlated mainly with relatively small-scale v-fluctuations and are synchronized well with the Q2 and Q4 motions. In the outer region, the correlation between very large-scale v and t fluctuations totally disappears, though the strong similarity between u and t remains. In the v-component, only relatively smaller-scale fluctuations may survive and contribute to the production of wall-normal turbulent heat flux vt, which is the primary turbulence quantity in heat transfer (for further details, see Nagano *et al.* 1995).

4. Turbulent transport associated with VITA events

The foregoing visual examination of simultaneous velocity and temperature traces has revealed qualitatively to what degree heat and momentum transfer is really governed by the coherent motions near the wall. There are several structural features in coherent motions. Among the most significant near the wall are the events detected with the VITA technique (Bogard & Tiederman 1987; Robinson 1991*b*). Thus, we

next examine the relationship between the VITA events and the heat and momentum transport. The VITA method is applied to the measurements in the buffer region ($y^+ = 18.5$). To further the discussion on coherent motions and their role in both heat and momentum transfer, we have used a so-called modified VITA technique supplemented with the slope criterion at a detection point, i.e. $du/d\tau$ (where τ is time). For the thresholds in the VITA technique, i.e. ku_{rms}^2 for the localized variance (Blackwelder & Kaplan 1976) and averaging time τ_{av}, we use $k = 1.2 \pm 0.4$ and τ_{av}^+ ($\equiv \tau_{av} u_\tau^2/\nu$) $= 9.5$, respectively.† The detected events have been analysed according to the classification of $du/d\tau > 0$ and $du/d\tau < 0$. The ratio of the number of VITA events thus obtained with $du/d\tau > 0$ to that with $du/d\tau < 0$ was 4.3 : 1, 7.6 : 1 and 12 : 1 for $k = 0.8$, 1.2 and 1.6, respectively. The dependency of this ratio on k has been investigated in detail by Johansson & Alfredsson (1982) and the present result accords well with their study. The difference in the ratio of the positive VITA events to the negative ones originates in the fact that near-wall coherent structures correspond mainly to positive VITA events ($du/d\tau > 0$). In the following, we show the results mainly for $k = 1.2$.

In figures 2(*a*) and 2(*b*), the ensemble-averaged patterns of the Reynolds shear stress, $-uv$, and streamwise and wall-normal turbulent heat fluxes, $-ut$ and vt, are shown together with u, v and t for each case of $du/d\tau > 0$ and $du/d\tau < 0$. The ensemble-averaging procedure is the same as that used in the conventional VITA method (Blackwelder & Kaplan 1976), in which all the detection points are brought into alignment at $\tau^+ = 0$. In figure 2, moreover, we have investigated the 'coherence in time' of the events by comparing two kinds of ensemble-averaged correlations, e.g. $-\langle uv \rangle$ and $-\langle u \rangle \langle v \rangle$. Here, a smaller difference between two conditionally averaged patterns means a higher coherence of the detected events, because background non-coherent motions survive more, for example, in the $\langle uv \rangle$-type averaging than in the $\langle u \rangle \langle v \rangle$-type‡.

As shown in figure 2(*a*), in the case of $du/d\tau > 0$, we see that $-\langle uv \rangle$, $-\langle ut \rangle$ and $\langle vt \rangle$ take respective local minima near the detection point ($\tau^+ = 0$) and show patterns similar to the twin peaks on both sides of $\tau^+ = 0$. Thus, heat and momentum transport by the VITA events is very small around the detection point, yet the coherent motions on both sides of this point transfer two or three times more heat and momentum than the relevant statistical averages (time averages), $-\overline{\hat{u}\hat{v}}(= -\overline{uv}/u_{rms}v_{rms})$, $-\overline{\hat{u}\hat{t}}$ and $\overline{\hat{v}\hat{t}}$. It should be noted that, under the condition of $du/d\tau > 0$, the coherent motions in the region $-10 < \tau^+ < 0$ can be regarded mostly as ejection-type (Q2) motions which are generally outward fluid motions with low velocity and high temperature, while those for $0 < \tau^+ < 10$ correspond mainly to the sweep-type (Q4) wallward motions with high velocity and low temperature. The profiles of $-\langle uv \rangle$ and $\langle vt \rangle$ are seen to be very similar to each other, which reflects the very analogous nature of both heat and momentum transfer near the wall (Nagano & Tagawa 1988; Iritani *et al.* 1985). Also,

† Appropriate determination of the threshold level for a detection scheme is always a matter of controversy. So, we have applied the values used in the representative works in the literature to the present study, i.e. the values of Blackwelder & Kaplan (1976) for (k, τ_{av}^+) in the VITA scheme. As discussed in the following, we have examined the sensitivities of the results to the various combinations of the threshold levels. This test showed that the essential features of the results remained unchanged even if the threshold levels are changed within the possible ranges. This also applies to the trajectory analysis technique in §5.1.

‡ Decomposing u and v as $u = \langle u \rangle + u'$ and $v = \langle v \rangle + v'$ leads to $\langle uv \rangle = \langle (\langle u \rangle + u')(\langle v \rangle + v') \rangle = \langle u \rangle \langle v \rangle + \langle u'v' \rangle$. Thus, the small difference between $\langle uv \rangle$ and $\langle u \rangle \langle v \rangle$ means that there is little correlation between u' and v', which thus can be regarded as random motions. In this case, the ensemble-averaged results $\langle u \rangle$ and $\langle v \rangle$ represent its turbulent structure and we term this state high coherence.

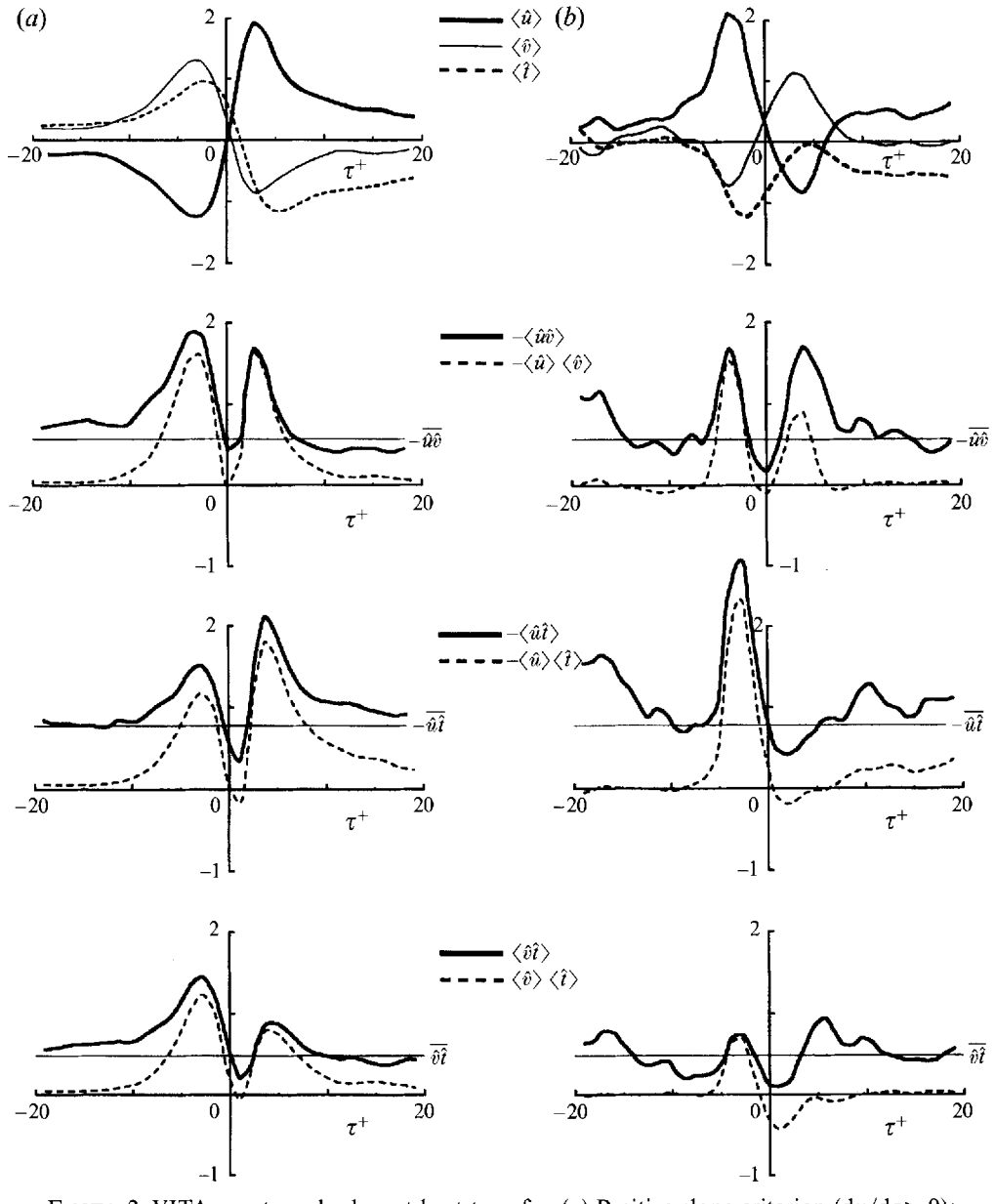

FIGURE 2. VITA events and relevant heat transfer. (*a*) Positive-slope criterion ($du/d\tau > 0$); (*b*) negative-slope criterion ($du/d\tau < 0$).

it can be seen that $-\langle ut\rangle$ peaks in the sweep phase ($\tau^+ > 0$), though $\langle vt\rangle$ becomes larger in the ejection phase ($\tau^+ < 0$). Hence, coherent motions are selective in their heat transfer actions. In addition, from comparison of $-\langle uv\rangle$ and $-\langle u\rangle\langle v\rangle$, $-\langle ut\rangle$ and $-\langle u\rangle\langle t\rangle$, and $\langle vt\rangle$ and $\langle v\rangle\langle t\rangle$, it can be concluded that coherent transport of heat and momentum lasts for $-10 < \tau^+ < 10$, and outside of this region non-coherent events serve to diminish heat and momentum transfer.

On the other hand, in the case of $du/d\tau < 0$ shown in figure 2(*b*), the $-\langle u\rangle\langle v\rangle$ profile shows that the organized momentum transfer by the negative-slope VITA events

($\mathrm{d}u/\mathrm{d}\tau < 0$) occurs only within $-5 < \tau^+ < 5$, and coherence in time itself is found to be very low because of the large difference between $-\langle uv \rangle$ and $-\langle u \rangle \langle v \rangle$ profiles. Furthermore, as mentioned previously, the number of detections is also very small, compared with the positive-slope VITA events ($\mathrm{d}u/\mathrm{d}\tau > 0$). These results mean that a negative-slope VITA event is not a main element of near-wall coherent structures. (Note that the roughnesses of the patterns in figure 2(*b*) is due to the small number of detections.) The manner in which the negative-slope VITA events contribute to turbulent heat transfer presents a marked contrast to that of the positive-slope VITA events. In other words, coherence in heat transfer can be observed only in the region $-5 < \tau^+ < 0$, whereas it disappears almost completely in the $0 < \tau^+ < 5$ region. In particular, the wall-normal heat flux $\langle vt \rangle$ is nearly equal to the statistical mean value $\overline{\hat{v}\hat{t}}$ all the time. For these reasons, the negative-slope VITA events are not the essential phenomena which dominate turbulent heat transfer in near-wall turbulence.

Here, we make some comments on the effects of the thresholds, k and τ_{av}, on the results shown in figure 2. If we change the value of k to $k = 1.2 \pm 0.4$, the peak values of $-\langle uv \rangle$, $-\langle ut \rangle$ and $\langle vt \rangle$ both in the $\tau^+ > 0$ and $\tau^+ < 0$ regions are increased by about $\pm 20\%$ for $\mathrm{d}u/\mathrm{d}\tau > 0$ and by $\pm 30\%$ for $\mathrm{d}u/\mathrm{d}\tau < 0$. These results are consistent with the findings by Blackwelder & Kaplan (1976) that the $\langle u \rangle$-patterns become universal when scaled by $(ku_{rms}^2)^{1/2}$. However, little effect of k on the temporal characteristics of $-\langle uv \rangle$, $-\langle ut \rangle$ and $\langle vt \rangle$ was seen for the range of $k = 0.8$–1.6. On the other hand, when τ_{av}^+ increases to 15.3 from 9.5, the pattern of $-\langle uv \rangle$ expands by about 30% in the direction of time since the time scale of a fluctuating component which we are looking at through the VITA technique changes with the averaging (integration) time τ_{av} (see Johansson & Alfredsson 1982). Thus, after investigating the effects of the thresholds on the results obtained, we have decided to use the threshold values of $k \approx 1.2$ and $\tau_{av}^+ \approx 10$, which are regarded as the standard ones in many applications of the VITA technique.

As made clear from the above analysis, if we use the ordinary VITA technique without slope criteria at a detection point, the two types of completely different phenomena shown in figures 2(*a*) and 2(*b*) may become inextricably mixed and thus there is no way to avoid contamination by misleading information on the coherent events. In fact, the ensemble averages obtained by the ordinary VITA technique without slope criteria (not shown here) indicate that values of $\langle u \rangle \langle v \rangle$, $\langle u \rangle \langle t \rangle$ and $\langle v \rangle \langle t \rangle$ become approximately half of the corresponding $\langle uv \rangle$, $\langle ut \rangle$ and $\langle vt \rangle$ values, which contrasts with the results shown in figure 2(*a*). Thus, the detected events become more incoherent than those of the positive-slope VITA events, although a decrease in order is not due to an increase of randomness but due to an intrusion of ordered motions with opposite properties. Consequently, the VITA technique with slope criteria should be used for analysis of transport phenomena in wall turbulence in order to prevent the elementary processes of coherent structures responsible for heat and/or momentum transfer from becoming contaminated with the negative-slope VITA events.

5. Trajectory analysis

5.1. *Trajectory analysis technique*

In a previous study, Nagano & Hishida (1990) developed a trajectory analysis technique by giving attention to the fact that the existence of coherent (well-ordered) motions can emerge with regularity in the trajectory on the (u, v)-plane because of the continuity of fluid motions, and they obtained several basic patterns of coherent

turbulent heat and momentum transfer. This technique can preserve information on the phase relation between the fluctuating components, u and v. In the present study, we refine the trajectory analysis technique by introducing two thresholds (h, H) to exclude the quadrant change triggered by unexpected noise-like components in signals. These thresholds enable the detection of only the important events playing a key role in coherent structures. As a result, accuracy and reliability in pattern recognition have become significantly higher than those of the previous technique of Nagano & Hishida (1990). The improved trajectory analysis technique (hereinafter referred to as TRAT) is composed of the following three steps. (i) Using the fluctuating velocity components u and v, fluid motions are classified into the four types, Qi ($i = 1, 2, 3, 4$), where i denotes the ith quadrant of the (u,v)-plane, in conformity with the quadrant splitting technique (Lu & Willmarth 1973). (ii) Obtain a time-series of quadrant sequences, Qi(1), Qi(2), $\cdots$, Qi(j), $\cdots$, where i changes with time according to the classification and j is an integer index which increases by one whenever a trajectory crosses a boundary of a quadrant of the (u,v)-plane. However, if the condition $|u(j)| \leqslant hu_{rms}$ and/or $|v(j)| \leqslant hv_{rms}$ is satisfied, Qi(j) is set to equal Qi($j-1$) to reject a meaningless quadrant change in the trajectory. (iii) The resultant time series of quadrants is decomposed and classified into a total of 36 patterns which are the permutations and combinations of three quadrants, Qi_1-Qi_2-Qi_3. In this processing, if the conditions $|uv(j-1)| \leqslant Hu_{rms}v_{rms}$, $|uv(j)| \leqslant Hu_{rms}v_{rms}$ and $|uv(j+1)| \leqslant Hu_{rms}v_{rms}$ are satisfied simultaneously, the pattern is discarded as an insignificant event unrelated to the coherent motions. The thresholds (h, H) are set to (h, H) = (0, 0) or (0.25, 0) or (0.25, 1.07) according to the objectives of the analysis. In the third combination of h and H, the value of $H = 1.07$ is determined from the finding of Bogard & Tiederman (1986) that ejections can be detected most accurately by the quadrant technique with this threshold level. On the other hand, for the first threshold h, a value of 0.25 is adopted on the basis of the modified u-level method (Luchik & Tiederman 1987), in which the detection algorithm has been constructed to mimic a so-called Schmitt trigger circuit: the detection function is turned on when $u \leqslant -Lu_{rms}$ (L: threshold) and turned off when $u \geqslant -0.25Lu_{rms}$. Luchik & Tiederman (1987) concluded that $L \approx 1$ is an adequate value to analyse the structure of ejections and bursts, which yields $h = 0.25$.

As an example, figure 3 shows how the pattern recognition is processed with the trajectory analysis technique (TRAT). If the TRAT without thresholds is applied, the trajectory of a turbulent motion shown in this figure is judged as Q4-Q3-Q2-Q3-Q2 (the underlined part is circled in figure 3) due to the existence of very small-scale fluctuations which can be neglected in the dynamics of coherent structures (Bogard & Tiederman 1986; Luchik & Tiederman 1987). The present scheme, however, can recognize this trajectory appropriately as Q4-Q3-Q2 by introducing the threshold, h. To know how adequately this threshold, h, works, we have applied the present TRAT to the u and v measurements mingled with white noise whose level is 0.1–0.2 times as high as the respective r.m.s. values of u and v. As a result, it has been confirmed that the pattern recognition was hardly affected by the white noise.

5.2. *Evaluation of VITA events using TRAT*

The VITA technique is a simple scheme in which the timescale and intensity of a phenomenon are used as criteria for detection. As shown in §4, however, the original VITA technique without the slope criterion equally detects phenomena which in reality have completely different characteristics in both heat and momentum transfer. Furthermore, even if the slope criterion is supplemented, there is no general guarantee

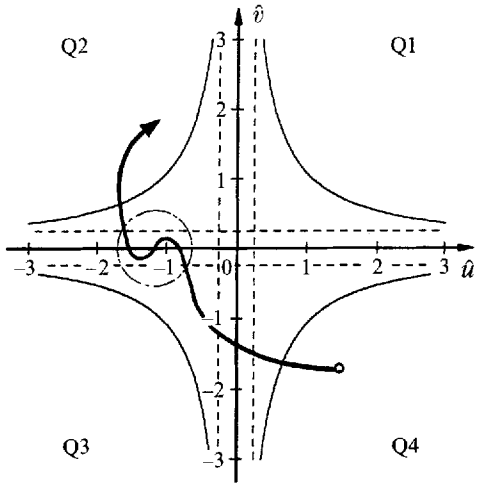

FIGURE 3. Trajectory analysis technique (TRAT) based on quadrant-sequences on the (u,v)-plane. ———, $H = 1.07$; − − − −, $h = 0.25$.

Pattern	%	Pattern	%
Q2-Q1-Q4	20.6	Q3-Q2-Q1	7.4
Q2-Q3-Q4	12.9	Q3-Q4-Q1	7.4
Q1-Q2-Q1	9.2	Q2-Q4-Q1	5.5
Q3-Q2-Q4	8.8	Q3-Q4-Q3	2.9
Q1-Q2-Q4	7.7	Q3-Q2-Q3	2.6

TABLE 2. Phase characteristics of the positive-slope VITA events.

that the phase relations among fluctuating components are maintained accurately in ensemble-averaged patterns. It should be remembered that the phase relation is extremely important in turbulent heat and momentum transfer since the Reynolds shear stress and turbulent heat fluxes are the products of velocity and temperature fluctuations, which often degenerate with increasingly mismatched phases. Thus, we have tried to make clear the phase characteristics of the VITA events by applying the TRAT to the events detected by the VITA-with-slope scheme. In this analysis, the thresholds were simply set to $(h,\ H) = (0,\ 0)$, because the detected VITA events were already large-scale coherent motions and further discrimination was not needed. Table 2 is a sample result at $y^+ = 18.5$. The numbers in table 2 show the ratios (in percentage) of occurrence of each pattern to the total number of positive-slope VITA events. The detection point of the VITA technique is located in the middle of each quadrant sequence. Here, only eight dominant patterns are presented. As seen from the table, although the positive-slope VITA events consist mostly of accelerative patterns such as Q2-Q1-Q4 and Q2-Q3-Q4 as expected, various other events with different phase characteristics are mixed with the VITA events. Thus, the important phase information will be lost even if the slope criterion is introduced into the original VITA technique.

The two accelerative patterns Q2-Q1-Q4 and Q2-Q3-Q4 are found to be dominant in the VITA events. Hence, to know their roles in heat and momentum transfer, we have performed ensemble averaging of the respective patterns. The results are shown

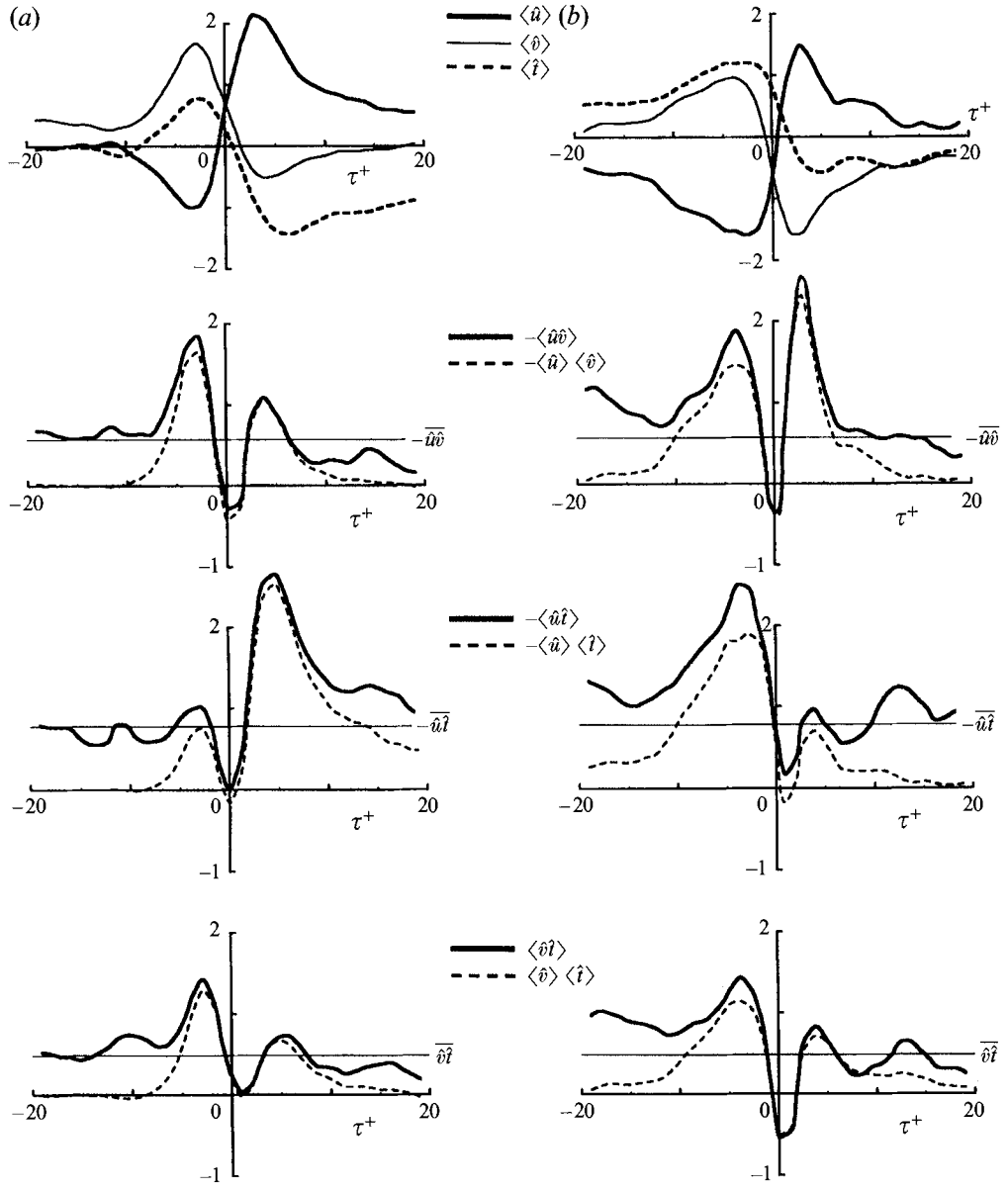

FIGURE 4. Flow and heat transfer characteristics in the positive-slope VITA events obtained with the TRAT. (*a*) Q2-Q1-Q4 pattern; (*b*) Q2-Q3-Q4 pattern.

in figures 4(*a*) and 4(*b*) in a similar manner as in figure 2. The detection point of the VITA technique is at $\tau^+ = 0$. Notable differences between ensemble averages in figures 4(*a*) and 4(*b*) are: (i) the contribution of Q4-motions ($\tau^+ > 0$) in the Q2-Q3-Q4 event to the production of the Reynolds shear stress is much higher than that in the Q2-Q1-Q4 event; (ii) the behaviour of axial turbulent heat flux $-\langle ut\rangle$ is completely different, depending on which accelerative pattern is involved, that is, the production of $-\langle ut\rangle$ is dominated by Q4-motions in the Q2-Q1-Q4 event but by Q2-motions in the Q2-Q3-Q4 event; (iii) around the detection point ($\tau^+ = 0$), the Q2-Q1-Q4 pattern

has no region of $\langle vt \rangle < 0$ but the Q2-Q3-Q4 clearly has a region of $\langle vt \rangle < 0$; and (iv) in the Q2 phase, coherence of the event Q2-Q3-Q4 is remarkably higher than that of the Q2-Q1-Q4 (see $\langle \cdot \rangle \langle \cdot \rangle$ quantities).

From the above analysis, it is evident that even the sophisticated VITA-with-slope technique recognizes essentially different phenomena in heat transfer to be the same events. In order to avoid this confusion, we need to detect and analyse coherent structures by keeping the correct phase information during the course of ensemble averaging. The present TRAT may afford the right key for the solution of the problem.

5.3. *Extraction of key patterns by TRAT*

Figure 5(*a*) shows sample results of the trajectories identified with the TRAT at $y^+ = 18.5$ in the buffer region where coherent motions are known to be most active. Firstly, the thresholds $(h, H) = (0, 0)$ are used in order to demonstrate the ultimate objectivity of the TRAT scheme. In figure 5, the detected frequency of occurrence of a trajectory Qi_1-Qi_2-Qi_3 is appended to the middle quadrant of the trajectory, i.e. Qi_2. For example, the frequency of occurrence of the trajectory Q4-Q1-Q2 is 550, which is thus appended to the first quadrant, Q1, of the (u,v)-plane. In the same manner, we may find that the frequencies of occurrence of Q4-Q1-Q4 and Q4-Q1-Q3 are 442 and 13, respectively. Thus, the sum of the events 'Q4 $\rightarrow$ Q1' is 1005 $(= 550 + 442 + 13)$, which originally comes from the sum of 610 Q1-Q4-Q1, 118 Q2-Q4-Q1 and 277 Q3-Q4-Q1 trajectories (the sum of these frequencies becomes 1005 as a matter of course). In figure 5(*a*), the total frequencies of occurrence of all 36 possible trajectories, N_{total}, was 7712. (Naturally, by simply dividing the numbers in figure 5(*a*) by N_{total}, the relative frequencies of occurrence are obtained, which should be independent of data length if N_{total} is sufficiently large.)

From figure 5(*a*), it is found that out of all 36 possible trajectories the patterns of Q3-Q4-Q3 (the frequency being 653), Q1-Q4-Q1 (610), Q4-Q3-Q2 (552), Q4-Q1-Q2 (550), Q2-Q3-Q4 (526), Q4-Q3-Q4 (483), Q1-Q2-Q1 (471), Q2-Q1-Q4 (470) and Q3-Q2-Q3 (460) occur very frequently in the near-wall region. On the other hand, Q3-Q1-Q3 (1), Q1-Q3-Q1 (2) and Q1-Q3-Q2 (4) rarely occur. However, to evaluate the fluid-dynamical importance of a trajectory, we need to sort out the trajectory based not only on the frequency of occurrence but also on its contribution to the statistics of turbulent quantities such as a fractional contribution to the Reynolds shear stress $\overline{uv}$. Thus, we have evaluated the contribution of each trajectory to the time-mean Reynolds stress $\overline{uv}$. The results of fractional contributions, $\langle uv \rangle / \overline{uv}$, are summarized in table 3 together with the frequencies of occurrence (number of events). In table 3, frequencies greater than 5% of N_{total} (386 in the $h = H = 0$ case) and fractional contributions greater than 10% of $\overline{uv}$ are underlined. It is seen from this table that a trajectory with a large frequency of occurrence is not necessarily a main contributor to $\overline{uv}$. For example, Q3-Q4-Q3 (653) and Q1-Q4-Q1 (610), whose frequencies are quite high, make a contribution to $\overline{uv}$ only of 6.2% and 5.8%, respectively. On the other hand, Q2-Q3-Q4 (526) and Q4-Q3-Q2 (552) make an outstanding contribution to $\overline{uv}$ of 33.5% and 29.8%, respectively. Thus, it can be concluded that only 8–10 trajectories out of 36 play an essential role in the dynamics of near-wall turbulence. From table 3, it is also evident that these important trajectories are also the main contributors to the turbulent heat flux $\overline{vt}$. Thus, turbulent heat transfer in the near-wall region is dominated almost always by the trajectories recognized as the turbulence-generating events. This implies that so-called Reynolds analogy between

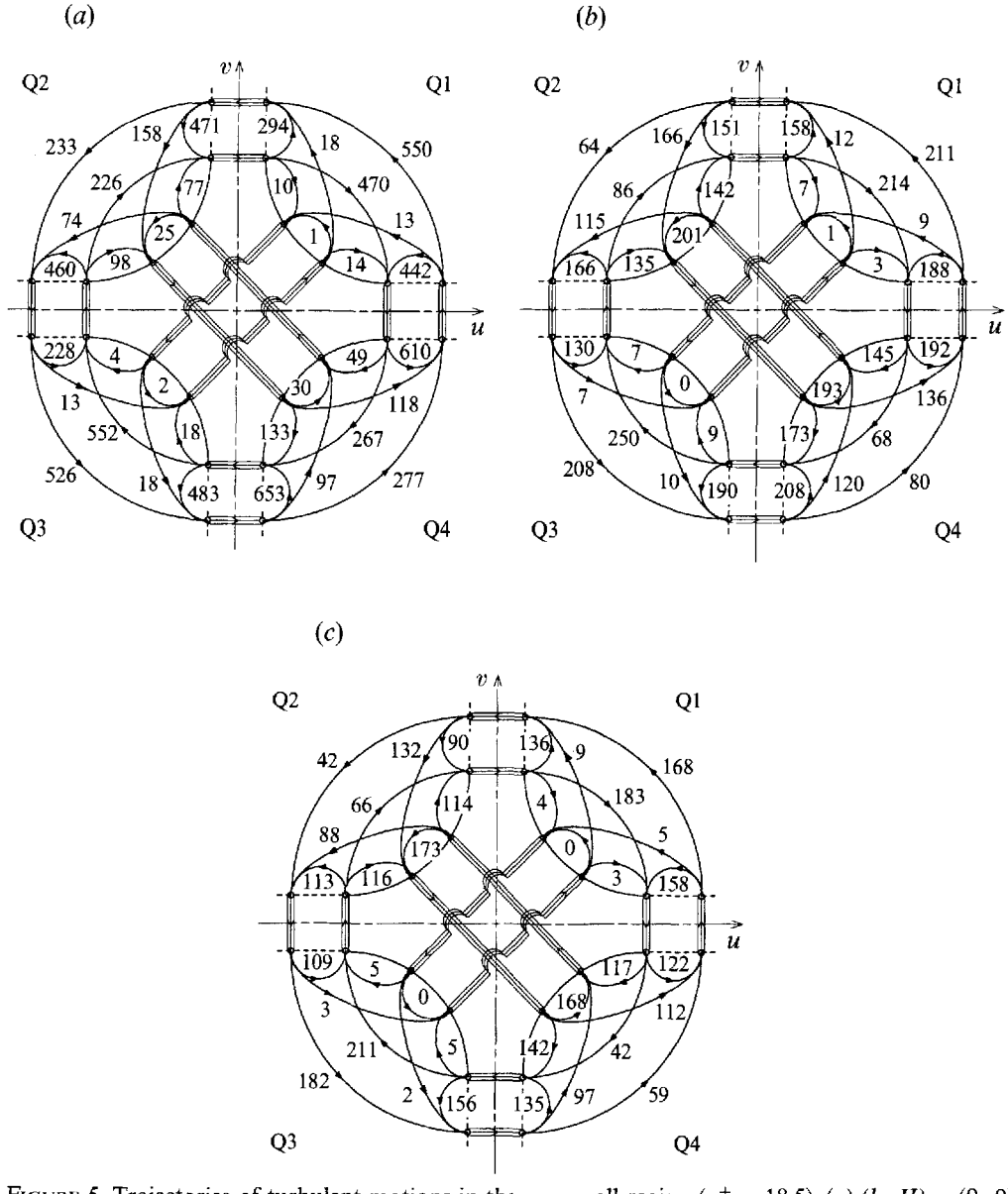

FIGURE 5. Trajectories of turbulent motions in the near-wall region ($y^+ = 18.5$). (*a*) $(h, H) = (0, 0)$, $N_{total} = 7712$; (*b*) $(h, H) = (0.25, 0)$, $N_{total} = 4155$; (*c*) $(h, H) = (0.25, 1.07)$, $N_{total} = 3267$.

heat and momentum transfer does hold even at this level if both velocity and thermal fields are fully developed (cf. Nagano *et al.* 1995).

Although the TRAT has the highest objectivity when $(h, H) = (0, 0)$, we can make much clearer the characteristics of each trajectory by introducing the threshold h into the TRAT. The results for $(h, H) = (0.25, 0)$ are shown in figure 5(*b*). In the case of $h \neq 0$, the total number of frequencies of occurrence of all trajectories decreased to 4155 from 7712, since some trajectories detected at $h = 0$ were united when $h \neq 0$ as illustrated in figure 3. The most remarkable change is seen in the frequencies of trajectories which contain a direct linkage of the Q2 and Q4 motions. For example, the frequencies of Q2-Q4-Q2 and Q4-Q2-Q4 have increased to 193 and 201 at $h = 0.25$

Trajectories Qi_1-Qi_2-Qi_3	$h = 0, H = 0$ Number of events	Contribution to $\langle uv\rangle/\overline{uv}$	Contribution to $\langle vt\rangle/\overline{vt}$	$h = 0.25, H = 1.07$ Number of events	Contribution to $\langle uv\rangle/\overline{uv}$	Contribution to $\langle vt\rangle/\overline{vt}$
Q1-Q2-Q1	471	0.084	0.095	90	0.040	0.043
Q1-Q2-Q3	233	0.091	0.079	42	0.033	0.031
Q1-Q2-Q4	158	0.084	0.073	132	0.116	0.109
Q1-Q3-Q1	2	0.000	0.000	0	0.000	0.000
Q1-Q3-Q2	4	0.000	0.000	5	0.010	0.009
Q1-Q3-Q4	18	0.004	0.006	2	0.000	0.000
Q1-Q4-Q1	610	0.058	0.072	122	0.034	0.043
Q1-Q4-Q2	49	0.029	0.030	117	0.103	0.109
Q1-Q4-Q3	267	0.045	0.068	42	0.021	0.031
Q2-Q1-Q2	294	0.197	0.213	136	0.168	0.183
Q2-Q1-Q3	10	0.002	0.002	4	0.000	0.001
Q2-Q1-Q4	470	0.227	0.237	183	0.151	0.165
Q2-Q3-Q1	13	0.002	0.003	3	0.001	0.000
Q2-Q3-Q2	228	0.209	0.229	109	0.169	0.181
Q2-Q3-Q4	526	0.335	0.276	182	0.217	0.189
Q2-Q4-Q1	118	0.018	0.019	112	0.111	0.101
Q2-Q4-Q2	30	0.031	0.027	168	0.228	0.219
Q2-Q4-Q3	133	0.076	0.080	142	0.130	0.135
Q3-Q1-Q2	18	0.003	0.003	9	0.004	0.005
Q3-Q1-Q3	1	0.000	0.000	0	0.000	0.000
Q3-Q1-Q4	14	0.001	0.001	3	0.001	0.002
Q3-Q2-Q1	226	0.091	0.120	66	0.056	0.074
Q3-Q2-Q3	460	0.149	0.151	113	0.091	0.088
Q3-Q2-Q4	98	0.062	0.062	116	0.116	0.115
Q3-Q4-Q1	277	0.075	0.066	59	0.036	0.029
Q3-Q4-Q2	97	0.046	0.040	97	0.091	0.082
Q3-Q4-Q3	653	0.062	0.047	135	0.028	0.026
Q4-Q1-Q2	550	0.234	0.196	168	0.140	0.115
Q4-Q1-Q3	13	0.002	0.002	5	0.003	0.004
Q4-Q1-Q4	442	0.178	0.200	158	0.124	0.141
Q4-Q2-Q1	77	0.039	0.034	114	0.097	0.098
Q4-Q2-Q3	74	0.033	0.026	88	0.090	0.083
Q4-Q2-Q4	25	0.017	0.017	173	0.217	0.215
Q4-Q3-Q1	18	0.002	0.002	5	0.000	0.001
Q4-Q3-Q2	552	0.298	0.314	211	0.229	0.247
Q4-Q3-Q4	483	0.180	0.183	156	0.110	0.117

TABLE 3. Summary of frequencies of occurrence and contributions to Reynolds shear stress $\overline{uv}$ and wall-normal turbulent heat flux $\overline{vt}$ for all 36 possible trajectories ($y^+ = 18.5$). Frequencies greater than 5% of N_{total} and fractional contributions greater than 10% of $\overline{uv}$ are underlined. (The key patterns are double-underlined.)

from 30 and 25 at $h = 0$, respectively. However, this is a natural consequence. That is, small-amplitude interactive Q1 and Q3 motions become discarded with increasing h values, so the original Q2-Q1-Q4 and Q2-Q3-Q4 patterns are in part identified as events with direct coupling of the Q2 and Q4 motions. Equally, the Q4-Q2 phase is composed mainly of the Q4-Q1-Q2 and Q4-Q3-Q2 patterns. Quantitative support to this conclusion will be given later (figure 7).

For further characterization of each trajectory, we have applied the thresholds $(h,\ H) = (0.25,\ 1.07)$ to the TRAT. The results are shown in figure 5(*c*). In this case, N_{total} becomes 3267. It should be noted that continuity in quadrant sequences, which holds in figures 5(*a*) and 5(*b*), is lost partly in the case of $H \neq 0$ since some trajectories not satisfying the criterion $|uv| > Hu_{rms}v_{rms}$ (with $H = 1.07$) were discarded. However, there is little noteworthy qualitative change in the frequencies of occurrence between the $H \neq 0$ (figure 5*c*) and $H = 0$ cases (figure 5*b*). To delineate a fluid-dynamical picture of coherent motions, on the other hand, the introduction of H is important as mentioned previously. Thus, in what follows, we will mainly focus on the results obtained under non-zero thresholds.

For all possible trajectories in the case $(h,\ H) = (0.25,\ 1.07)$, the frequencies of occurrence and the contributions to $\overline{uv}$ and $\overline{vt}$ are also summarized in table 3. From this table, we may classify the important trajectories into two categories: one is the trajectory which has an interaction, Q1 or Q3, between the Q2 and Q4 motions, i.e. Q2-Q1-Q4, Q2-Q3-Q4, Q4-Q1-Q2 and Q4-Q3-Q2; and the other is the trajectory which has an interaction dividing the Q2 or Q4 event into two parts such as Q2-Q1-Q2, Q2-Q3-Q2, Q4-Q1-Q4 and Q4-Q3-Q4. The trajectories in the first category appear at the interface between ejection- and sweep-type motions and correspond well to the VITA events. Thus, these trajectories represent the essential features of near-wall turbulence, so we call these the 'key patterns'. These key patterns are double-underlined in table 3. Obviously, from the results at both $(h,\ H) = (0,\ 0)$ and $(h,\ H) = (0.25,\ 1.07)$, one can see that the key patterns stand out as special: the number of event occurrences is very large and their contributions to $\overline{uv}$ and $\overline{vt}$ are also outstandingly large.

On the other hand, the trajectories belonging to the second category may appear when either the u- or v-component has monotonic fluctuations with large timescales. As will be shown later (figure 8), these trajectories have features quite different from the key patterns, and do not contain the strong Q2 and Q4 motions corresponding clearly to the ejection- and sweep-type motions. Thus, we call these trajectories the 'sub-patterns' whose contribution to $\overline{uv}$ cannot be neglected.

To assess the soundness of the present TRAT and the reliability of the detected results, we have examined the following three points under the same threshold condition of $(h,\ H) = (0.25,\ 1.07)$: (i) trajectory pattern distributions identified in computer-generated pseudo-turbulence which has u- and v-components conforming to the joint Gaussian p.d.f. with $\overline{\hat{u}\hat{v}} = \overline{uv}/(\overline{u^2})^{1/2}(\overline{v^2})^{1/2} = 0$ or -0.5; (ii) changes in detected pattern distributions with a location from the buffer region ($y^+ = 18.5$) to the outer layer ($y^+ = 192$) or the turbulent core ($y^+ = 385$); and (iii) pattern-distribution changes with different threshold levels, h and H. Although the figures are not shown here, the results can be summarized briefly as follows. When the Gaussian random numbers with $\overline{\hat{u}\hat{v}} = 0$ were input to the TRAT instead of the actual fluctuating velocity components u and v, the total number of detected patterns became about six times as large as real ones at $y^+ = 18.5$, and the occurrence ratio of 2.1% for each pattern, when normalized by N_{total} at $(h,\ H) = (0.25,\ 0)$, was almost the same through all 36 possible patterns (the sum of the ratios does not reach 100% because $H \neq 0$). On the other hand, when the Gaussian random numbers simulating a non-isotropic turbulence field ($\overline{\hat{u}\hat{v}} = -0.5$) were used, the total number of pattern occurrences was also about six times that actually detected at $y^+ = 18.5$. However, a significant bias was seen in the pattern distributions; the negative correlation between u and v increased the occurrence ratio of the patterns Q2-Q4-Q2 (10.2%) and Q4-Q2-Q4 (10.3%), and a marked decrease was observed in occurrence of patterns which

include the Q1- and Q3-motions. As for the key patterns extracted from figure 5, their occurrence ratios in pseudo-turbulence with $\overline{\hat{u}\hat{v}} = -0.5$ became 2.2%, 2.5%, 2.3% and 2.6% for Q2-Q1-Q4, Q2-Q3-Q4, Q4-Q1-Q2 and Q4-Q3-Q2, respectively, which was essentially the same as in the case of $\overline{\hat{u}\hat{v}} = 0$ (2.1%). This is the most important phenomenological difference between the actual wall turbulence and the pseudo-turbulence. This difference is due to the spatio-temporal continuity of actual turbulent motions and the existence of coherent structures near the wall. This in turn indicates that the present TRAT works appropriately to detect the coherent motions, if any.

In the outer and core regions, the total number of pattern occurrences was 1.5 times that in the buffer region, and the Q4-Q1-Q4 and Q2-Q3-Q2 patterns slightly increased. In these regions, however, the obvious superiority of the key coherent patterns near the wall disappeared and their occurrence ratios decreased to those in pseudo-turbulence of $\overline{\hat{u}\hat{v}} = -0.5$. This result means a substantial loss of well-ordered turbulent structures. On the other hand, comparison between the results in the wall region for $h = 0$ and those for $h = 0.25$ at $H = 1.07$ showed that the total number of pattern occurrences at $h = 0.25$ decreased by 46% and the direct connection of Q2- and Q4-motions (Q2 → Q4 or Q4 → Q2) became pronounced (ten times as large), indicating that weak interactive motions insignificant in the dynamics of wall turbulence had been removed. The key coherent patterns Q2-Q1-Q4, Q2-Q3-Q4, Q4-Q1-Q2 and Q4-Q3-Q2, however, decreased by only 30% with an increase of h. This clearly shows that these key patterns are the flow phenomena with strong interactive motions Q1 and Q3 in between, and with distinct phase characteristics. It should also be mentioned that no important changes were observed in the essential characteristics of any pattern even though the threshold h had changed.

Although strict definition of the coherent structures is a very demanding task, it is clear that tracking an event both in three-dimensional space and in time should be the best way of identifying its structure. However, the existence of coherent structures should also be reflected in the time-series trajectory of the velocity components measured at one point in space. Of course, their footprints would not be very clear due to their inherent ambiguity and the existence of background turbulence, but they are detectable by making the TRAT scheme as objective as possible. As illustrated in figure 5(*a*), there is actually some skewness in the frequency of occurrence, which is never observed if the flow field is a totally random system. We should also mention that we have recognized the four distinct patterns in the sequence of coherent motions (Nagano & Hishida 1990) as Q4-Q1-Q2-Q1-Q4, Q4-Q1-Q2-Q3-Q4, Q4-Q3-Q2-Q3-Q4, and Q4-Q3-Q2-Q1-Q4 after investigating all possible trajectories on the (u, v)-plane. These four patterns have a marked higher frequency of occurrence than the rest of all possible combinations. And, needless to say, the four key patterns identified here, i.e. Q2-Q1-Q4, Q2-Q3-Q4, Q4-Q1-Q2 and Q4-Q3-Q2 are the elements of the above-mentioned four distinct patterns with the deterministic regularity in sequences of events.

From the above analyses, the four patterns Q2-Q1-Q4, Q2-Q3-Q4, Q4-Q1-Q2 and Q4-Q3-Q2 can be considered to be the key flow patterns of the coherent motions in wall turbulence. In order to obtain further details of the characteristics of the important trajectories in heat and momentum transport, we have performed an ensemble averaging of them with the procedure of Nagano & Hishida (1990), a scheme which can hold phase information between the fluctuating components of u and v. The procedure in the TRAT consists of the following steps: (i) to extract fluid motions which belong to a specified pattern; (ii) to calculate the mean duration for

each quadrant of the pattern; and (iii) to perform ensemble averaging by adjusting the temporal duration of each event to the mean duration of the respective Qi motions while keeping the phase relations between u and v. We can formulate this procedure as follows:

$$\langle\chi(\tau)\rangle \text{ for } Qi_1\text{-}Qi_2\text{-}Qi_3 = \begin{cases} \dfrac{1}{N}\displaystyle\sum_{n=1}^{N}\chi\left(r_{1,n}\,\tau+\tau_{o1,n}\right) & \text{for } Qi_1\text{-motion,} \\ \dfrac{1}{N}\displaystyle\sum_{n=1}^{N}\chi\left(r_{2,n}\,\tau+\tau_{o2,n}\right) & \text{for } Qi_2\text{-motion,} \\ \dfrac{1}{N}\displaystyle\sum_{n=1}^{N}\chi\left(r_{3,n}\,\tau+\tau_{o3,n}\right) & \text{for } Qi_3\text{-motion,} \end{cases} \tag{5.1}$$

where χ denotes a fluctuating component, τ is time, N is the number of occurrences of the pattern Qi_1-Qi_2-Qi_3, n is a label number which increases by one when the TRAT detects a fluid motion belonging to the specified pattern, $r_{i,\,n}$ is an adjusting factor for the ensemble averaging defined as $r_{i,\,n} = \Delta T_{i,\,n}/\overline{\Delta T_i}$ ($\Delta T_{i,n}$ denotes the individual duration of the Qi motions of the pattern labelled n, and $\overline{\Delta T_i}$ is the mean duration of the Qi motions of the pertinent pattern. Thus, $\overline{\Delta T_i} = (1/N)\sum_{n=1}^{N}\Delta T_{i,\,n}$), and τ_{o1}, τ_{o2} and τ_{o3} are the reference points in time when Qi_1-, Qi_2- and Qi_3-motions of the Qi_1-Qi_2-Qi_3 pattern begin, respectively.

Figure 6(*a*) shows the ensemble-averaged patterns of Q2-Q1-Q4 and Q2-Q3-Q4. As seen in figure 6(*a*), the ensemble-averaged streamwise velocity fluctuation $\langle u\rangle$ represents the typical u-signal pattern of near-wall turbulence, which consists of a gradual deceleration from a local maximum followed by a strong acceleration (Wallace *et al.* 1977). In response to this motion, a temperature front characterized by a steep decrease of temperature and related deeply to the turbulent burst (Chen & Blackwelder 1978; Subramanian *et al.* 1982; Antonia *et al.* 1982) is seen in the $\langle t\rangle$-pattern. Thus, these patterns are representative of the phenomena existing in wall turbulent shear flows. Furthermore, all the important features seen in the accelerating patterns of the VITA events with $\mathrm{d}u/\mathrm{d}\tau > 0$ (figure 4) are also observed in figure 6(*a*).

On the other hand, through comparison of the decelerating patterns between Q4-Q1-Q2 and Q4-Q3-Q2 (figure 6*b*), the following differences are found: (i) the duration of Q4-Q1-Q2 is shorter than that of Q4-Q3-Q2; (ii) the Q2- and Q4-motions in the Q4-Q1-Q2 and Q4-Q3-Q2 patterns contribute quite differently to the streamwise turbulent heat flux, $-\langle ut\rangle$; and (iii) remarkable productions of $-\langle uv\rangle$ and $\langle vt\rangle$ occur during the Q2-motion of Q4-Q3-Q2. The Q4-Q3-Q2 pattern is especially important because it is always accompanied by the strong ejections responsible for the dynamics of wall turbulence.

The ensemble-averaged patterns of Q2-Q4-Q2 and Q4-Q2-Q4 are given in figure 7 to show that these patterns are basically composed of the key patterns. It is seen from this figure that the $\langle u\rangle$- and $\langle v\rangle$-fluctuations in the first half of Q2-Q4-Q2, i.e. the Q2 $\rightarrow$ Q4 phase, show just the averaged characteristics of Q2-Q1-Q4 and Q2-Q3-Q4. Similarly, those in the later half, the Q4 $\rightarrow$ Q2 phase, are depicted by the average of Q4-Q1-Q2 and Q4-Q3-Q2. From figure 7 and table 3, it is concluded that most of the Q2-Q4-Q2 and Q4-Q2-Q4 events detected at $h = 0.25$ were composed originally of the four key patterns and the essential features of Q2-Q4-Q2 and Q4-Q2-Q4 can

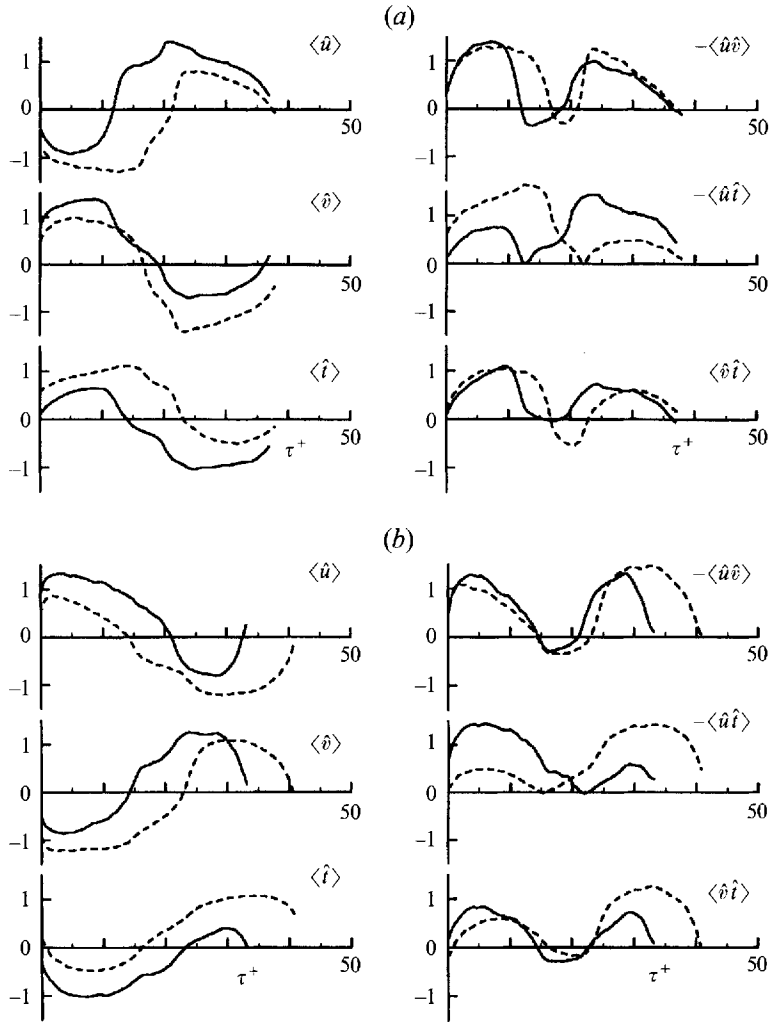

FIGURE 6. Ensemble-averaged characteristics of turbulence quantities in velocity and thermal fields obtained with the TRAT ($y^+ = 18.5$). (*a*) Accelerative patterns: ———, Q2-Q1-Q4; – – – –, Q2-Q3-Q4; (*b*) decelerative patterns: ———, Q4-Q1-Q2; – – – –, Q4-Q3-Q2.

be represented by the four key patterns. Thus, we need not add these trajectories to the key patterns.

Figure 8 shows the ensemble-averaged patterns of Q2-Q1-Q2, Q2-Q3-Q2, Q4-Q1-Q4 and Q4-Q3-Q4, which were categorized as sub-patterns. As shown in figure 8(*a*), the Q2-Q1-Q2 and Q2-Q3-Q2 trajectories, which are Q2-based sub-patterns, are quite different from each other depending on which interaction, Q1 or Q3, divides the Q2 motion. Particularly, the Q2-Q3-Q2 pattern is not detected by the VITA technique because of the quite gentle behaviour of $\langle u\rangle$. Responding to this, $\langle t\rangle$ of Q2-Q3-Q2 is kept consistently at high temperature. These unique characteristics have been observed in the low-speed streaks near the wall using a technique of simultaneous visualization of velocity and thermal fields (Iritani *et al.* 1985). On the other hand, the ensemble-averaged Q4-Q1-Q4 and Q4-Q3-Q4 patterns, i.e. Q4-based sub-patterns, have nearly the same timescales, and there is a weak but perceptible similarity in $\langle u\rangle$, $\langle v\rangle$ and $\langle t\rangle$. Consequently, no substantial differences between Q4-Q1-Q4 and Q4-Q3-Q4

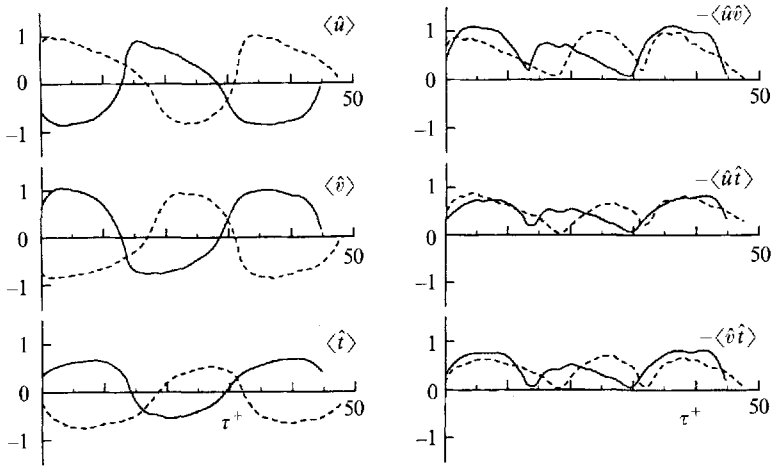

FIGURE 7. Ensemble-averaged characteristics of turbulence quantities of the Q2-Q4-Q2 and Q4-Q2-Q4 patterns ($y^+ = 18.5$). ———, Q2-Q4-Q2; – – – –, Q4-Q2-Q4.

patterns are seen in $\langle uv\rangle$ and $\langle vt\rangle$. The most remarkable difference, however, is found in the amount of streamwise turbulent heat flux $\langle ut\rangle$.

Meanwhile, there is a possibility that other patterns important in heat transfer are hidden, so we need to find another way of evaluating a pattern from the standpoint of heat transfer. Thus, by focusing on the ejections (Q2-motions) dominating all the transport processes (Nagano & Tagawa 1988), we have extracted patterns contributing to turbulent heat transfer through the following equation:

$$\left[\overline{\hat{v}\hat{t}}\right]_{Q2} = \frac{1}{T}\int_0^T \hat{v}(\tau)\,\hat{t}(\tau)\,I\,[Qi(\tau)=Q2]\mathrm{d}\tau \text{ for any specified } Qi_1\text{-}Qi_2\text{-}Qi_3 \text{ motion,} \tag{5.2}$$

where $I\,[Qi(\tau)=Q2]$ is the detection function which is unity if the component Qi of the specified pattern Qi_1-Qi_2-Qi_3 becomes Q2 and is zero otherwise. Equation (5.2) may give an objective evaluation for the contribution of each Q2-motion to $\overline{vt}$.

The patterns Q4-Q3-Q2 (0.0866), Q2-Q3-Q4 (0.0687) and Q3-Q2-Q3 (0.0608) detected at (h, H) = (0.25, 1.07) are found to contain the important Q2-motions contributing largely to turbulent heat transfer at $y^+ = 18.5$. Numerical values in parentheses indicate the values obtained from (5.2), and the relative contributions of each pattern to the overall turbulent heat transfer can be evaluated by comparing these values with a time average $\overline{\hat{v}\hat{t}} = \overline{vt}/v_{rms}t_{rms} = 0.48$ for $I \equiv 1$. From this analysis, it becomes evident that the Q3-Q2-Q3 pattern, though occurring less frequently (the frequency is 113) than other dynamically important patterns shown in figure 5(c), makes a very large contribution to turbulent heat transfer near the wall. This type of event is hardly detected by the VITA technique, so is not suited to reveal the characteristics of this type of coherent heat transfer.

A similar analysis has been done for momentum transfer to quantify the contributions of the principal patterns to the magnitude of Reynolds shear stress $-\overline{uv}$ just like (5.2) for $\overline{vt}$. The results are summarized in table 4 for the important nine trajectories (values in the table show the fractional contribution of each quadrant motion, normalized by $\overline{uv}$). From the table, we can extract the most important three patterns whose Q2 motion shows a large contribution to $-\overline{uv}$, underlined in table 4. They are

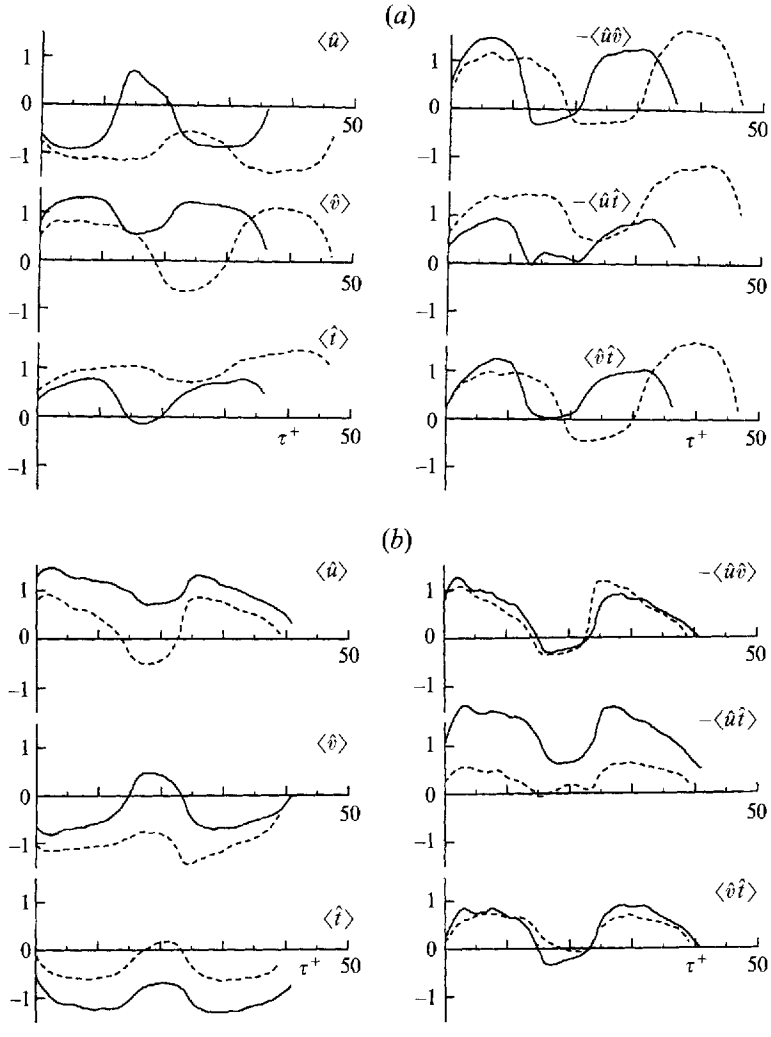

FIGURE 8. Ensemble-averaged characteristics of turbulence quantities of sub-patterns ($y^+ = 18.5$). (*a*) Q2-based sub-patterns: ———, Q2-Q1-Q2; – – – –, Q2-Q3-Q2; (*b*) Q4-based sub-patterns: ———, Q4-Q1-Q4; – – – –, Q4-Q3-Q4.

Q4-Q3-Q2, Q2-Q3-Q4 and Q3-Q2-Q3. This means that the Q3-Q2-Q3 pattern is very important not only in heat transfer but also in the fluid dynamics.

The ensemble-averaged heat and momentum transfer in the Q3-Q2-Q3 pattern is shown in figure 9. Evidently, the Q3-Q2-Q3 event is quite different from the four key patterns shown in figure 6. Although this pattern cannot be detected at all by the VITA method, a great deal of turbulent heat and momentum transfer occurs in the Q2-phase of this pattern.

Here, it should be emphasized that all of the above-mentioned key patterns exhibit only small differences in the two kinds of ensemble-averaged correlations mentioned in §4, e.g. $-\langle uv\rangle$ and $-\langle u\rangle\langle v\rangle$ (figures not shown here). This provides further evidence that the present TRAT can maintain the phase relations between the fluctuating components u, v and t, and that the coherence of the detected events is considerable. (In the VITA technique, coherence of events is easily contaminated during the ensemble-averaging stage.)

Trajectories Qi_1-Qi_2-Qi_3	Contribution to $\langle uv\rangle/\overline{uv}$ $h = 0.25, H = 1.07$			
	Qi_1	Qi_2	Qi_3	Total
Q2-Q1-Q4	0.095	−0.012	0.068	0.151
Q2-Q3-Q4	0.142	−0.009	0.084	0.217
Q4-Q1-Q2	0.077	−0.011	0.074	0.140
Q4-Q3-Q2	0.081	−0.019	0.167	0.229
Q2-Q1-Q2	0.090	−0.009	0.087	0.168
Q2-Q3-Q2	0.087	−0.013	0.095	0.169
Q4-Q1-Q4	0.076	−0.010	0.058	0.124
Q4-Q3-Q4	0.057	−0.015	0.068	0.110
Q3-Q2-Q3	−0.014	0.116	−0.011	0.091

TABLE 4. Contribution of each quadrant motion (Qi) of the important trajectories to the magnitude of the Reynolds shear stress. All values are normalized by the time-mean value $\overline{uv}$.

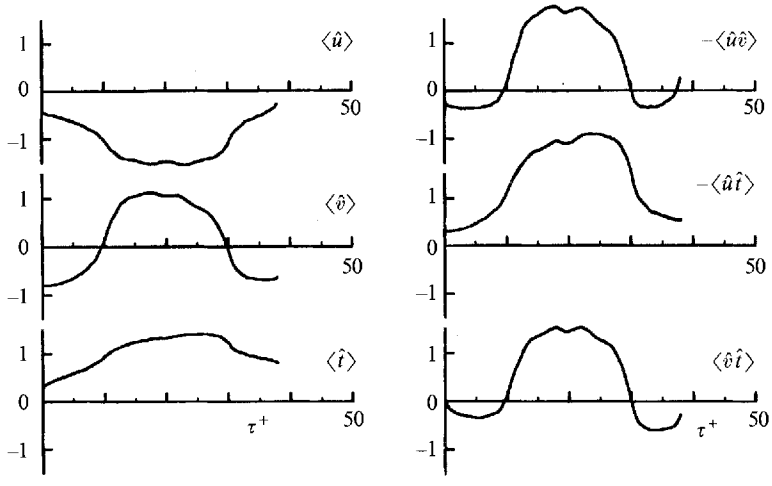

FIGURE 9. Ensemble-averaged structures of Q3-Q2-Q3 pattern contributing significantly to turbulent heat transfer ($y^+ = 18.5$).

As mentioned repeatedly, to make clear the relationship between the key flow patterns and heat transfer, information obtained from the ensemble-averaged patterns of velocity and temperature fluctuations by keeping a strict phase relationship is very important. For example, it is revealed that there are remarkable differences in the behaviour of turbulent heat fluxes $\langle ut\rangle$ and $\langle vt\rangle$, as shown in figure 6, between the key patterns. These differences are much larger than those conceivable from their trajectories (see also figure 12). Thus, it can be said that these ensemble-averaged patterns represent the essential characteristics of heat transport in wall turbulence, and the present TRAT is the first to identify such important characteristics of turbulent heat transfer.

5.4. *Correspondence of TRAT results with flow isualization measurements*

Since it may be impossible to reveal the entire nature of the turbulence structures solely with one detection method, we need to analyse the coherent structures by using a combination of various detection schemes and examining the data from different

points of view as done by Bogard & Tiederman (1986), Morrison, Tsai & Bradshaw (1989) and Spina *et al.* (1991). The present TRAT is designed to evaluate a fluid motion (turbulence structure) rather than only to detect an event. In this respect, the TRAT is applicable to the analysis of the structures extracted from, for example, PIV/PTV and DNS databases to identify the phase characteristics of a particular structure and to make clear quantitatively the transport phenomena of heat and momentum associated with the structure. Thus, it is of primary importance to extract key flow patterns from the trajectories obtained by the TRAT, and to investigate the dynamical aspects of the patterns and their relevant transport phenomena.

Based on flow visualization experiments, Bogard & Tiederman (1987) have revealed that ejections, which are the core motions in coherent structures in wall turbulence, yield different velocity characteristics depending on different phase alignment (i.e. leading edge, middle and trailing edge), and they obtained the ensemble-averaged patterns $\langle u \rangle$, $\langle v \rangle$ and $\langle uv \rangle$ for each. To determine whether the present TRAT results correspond to those of these three parts of ejections, we performed ensemble averaging for each pattern detected by TRAT at the midpoint of the second quadrant without phase alignment, so as to coincide with the scheme of Bogard & Tiederman (1987). Then, we compared the present results ($y^+ = 18.5$) with those of their flow visualization experiments ($y^+ = 15$) (Bogard & Tiederman 1987; Luchik & Tiederman 1987).

This careful search for correspondence revealed that the three parts of ejections (i.e. leading edge, middle and trailing edge) correspond to the patterns Q4-Q3-Q2, Q3-Q2-Q3 and Q2-Q3-Q4, respectively. Figure 10 shows the remarkably good correspondence between the $\langle u \rangle$ patterns obtained by the flow visualization experiment (dashed lines) and those by the TRAT (solid lines). Namely, both the amplitude and the timescale of $\langle u \rangle$ in the experiment of Bogard & Tiederman (1987) are in excellent agreement with those obtained by the present TRAT. It should be noted here that, as shown in §5.3, the patterns Q4-Q3-Q2, Q3-Q2-Q3 and Q2-Q3-Q4 are detected by the present TRAT as the important trajectories in the near-wall region (two of which, i.e. Q4-Q3-Q2 and Q2-Q3-Q4, belong in fact to the key patterns). This implies that these trajectories must be the reflections of the three parts of ejections which are the dominant events near the wall (Bogard & Tiederman 1987).

The corresponding heat and momentum transfer associated with the Q4-Q3-Q2, Q3-Q2-Q3 and Q2-Q3-Q4 patterns (figure 10) are shown in figure 11. Obviously, marked heat transfer is found to occur in the middle of ejections related to the Q3-Q2-Q3 pattern. Note that this finding is consistent with that derived from (5.2) with the TRAT (see figure 9).

Although it may be necessary to ensemble average the detected events in spatial alignment to reveal the entire nature of a particular structure, it is now increasingly acknowledged in the turbulence research community that we need some technique and guideline to analyse the huge amount of data provided by DNS or image velocimetry such as PIV/PTV. The TRAT may contribute to the detailed investigation and evaluation of a particular structure extracted from the database using various detection scheme. As shown in the above, the TRAT can coexist with other analysis methods to identify a structure more objectively and to reveal the essential features of corresponding transport phenomena.

5.5. *Vector maps of heat and momentum transfer*

The characteristics of each pattern shown in figures 6 and 9 can be made more clear by arranging in sequential order the temporal data of the coherent velocity vector

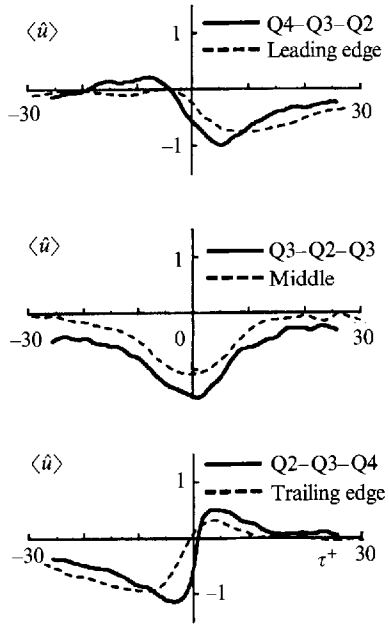

FIGURE 10. Correspondence of ensemble-averaged velocity fluctuations (solid lines) with flow visualization measurements of Bogard & Tiederman (1987) (dashed lines).

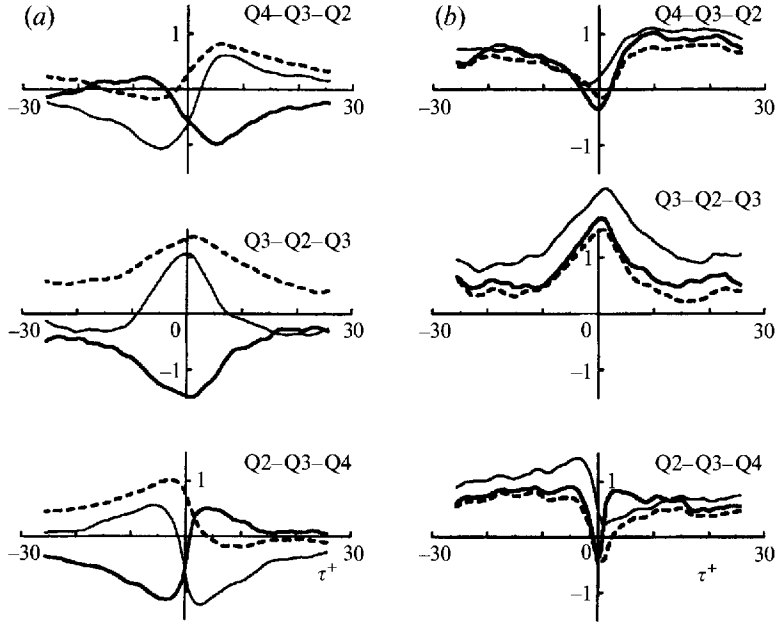

FIGURE 11. Ensemble-averaged characteristics of heat and momentum transfer corresponding to the flow visualization experiment of Bogard & Tiederman. (*a*) Fluctuating components $\langle u \rangle$, $\langle v \rangle$ and $\langle t \rangle$: ——, $\langle u \rangle$; ——, $\langle v \rangle$; – – – –, $\langle t \rangle$; (*b*) Reynolds shear stress and turbulent heat fluxes $-\langle uv \rangle$, $-\langle ut \rangle$ and $\langle vt \rangle$: ——, $-\langle uv \rangle$; ——, $-\langle ut \rangle$; – – – –, $\langle vt \rangle$.

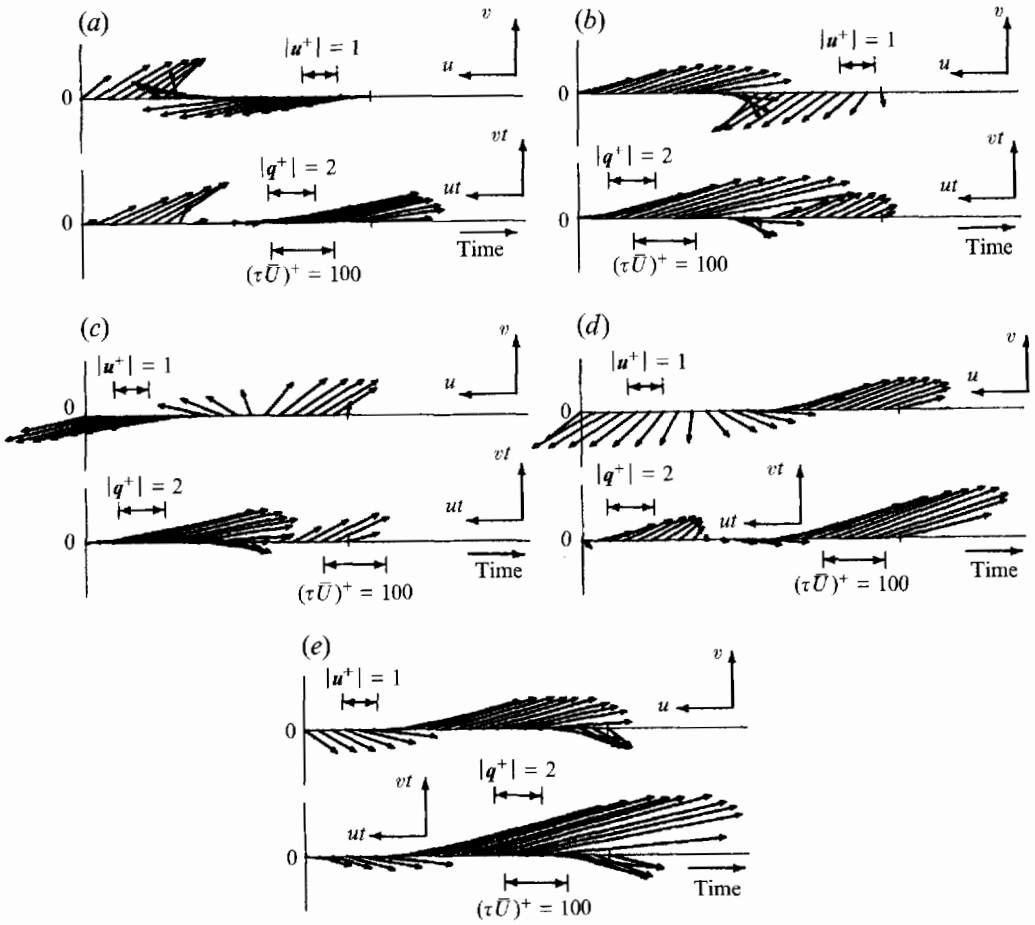

FIGURE 12. Vector maps of velocity and thermal fields for key flow patterns identified by the TRAT. (*a*) Q2-Q1-Q4; (*b*) Q2-Q3-Q4; (*c*) Q4-Q1-Q2; (*d*) Q4-Q3-Q2; (*e*) Q3-Q2-Q3.

$\boldsymbol{u} = \langle u \rangle\, \boldsymbol{i} + \langle v \rangle\, \boldsymbol{j}$ and the relevant turbulent heat-flux vector $\boldsymbol{q} = \langle ut \rangle \boldsymbol{i} + \langle vt \rangle \boldsymbol{j}$ ($\boldsymbol{i}$ and $\boldsymbol{j}$ denote the unit vectors in the streamwise and wall-normal directions, respectively). Figure 12(*a–e*) shows these vector maps for each key pattern in the buffer region ($y^+ = 18.5$). Here, velocity and temperature fluctuations are normalized by the friction velocity u_τ and friction temperature t_τ, respectively.

From the vector maps of $\boldsymbol{u}$ shown in figures 12(*a*) and 12(*b*), it can be seen that fluid motions of the Q2-Q1-Q4 and Q2-Q3-Q4 patterns are quite different, though both are similar accelerating motions. The Q2-Q3-Q4 pattern exhibits a penetration-like motion toward the wall in the sweep phase in contrast with the Q2-Q1-Q4 pattern. Strong interference between the Q2- and Q4-motions is seen in the interaction phases of both patterns, where a great deal of turbulence dissipation occurs. (The ensemble-averaged patterns of $(\mathrm{d}u/\mathrm{d}\tau)^2$, which correspond to turbulence dissipation (Nagano & Hishida 1985), had large peak values only in these narrow regions of interaction (figures not shown).)

The velocity vector maps of the decelerating patterns Q4-Q1-Q2 and Q4-Q3-Q2 (figure 12*c* and 12*d*) also display remarkable differences. For example, concentrations of the velocity vectors in the Q2- and Q4-motions of the Q4-Q1-Q2 pattern are

completely opposite to those of Q4-Q3-Q2. These differences seem much larger than those conceivable from the ensemble-averaged patterns in figure 6(*b*). Figure 12(*e*) shows the velocity vector map of the Q3-Q2-Q3 pattern whose Q2-motions contribute significantly to turbulent heat transfer. Evidently, this pattern has no flow interference as seen in the accelerating patterns. As mentioned previously, the pattern can be viewed as the middle stage in the ejections (figure 10).

On the other hand, as seen in the $\boldsymbol{q}$ vector maps for patterns Q2-Q1-Q4 and Q2-Q3-Q4 (figures 12*a* and 12*b*), turbulent heat transport during Q2-Q1-Q4 occurs more intermittently than with Q2-Q3-Q4. The amount of heat transported by the Q2-motions (ejection-phase) becomes large in the events Q2-Q3-Q4, Q4-Q3-Q2 and Q3-Q2-Q3. This result is identical to the evaluated contributions of the Q2-motions of each pattern to the time-averaged turbulent heat transfer (§5.3). Especially, the Q2-motions of the Q3-Q2-Q3 pattern accompany a large amount of heat transport.

6. Statistical time-series prediction of coherent heat transfer using the autoregressive model

If we consider a turbulent transport phenomenon to be a statistical dynamic system, we can get useful information on the prediction and control of turbulence by applying various mathematical theories to the analysis of this system. Convective heat transfer in incompressive fluids can be expressed mathematically as a statistical dynamic system whose inputs are the fluctuating velocity components u and v and output is the temperature fluctuation t. (Since the lateral velocity component, w, is a variable dependent on u and v, only the u- and v-components are treated as the input variables.) The autoregressive (AR) model may be useful to find the realizability of the key flow patterns detected by the present TRAT and to find how heat transport is induced by these flow patterns.

Let $X(s)$ be a k-dimensional, stationary time series: $X(s) = (x_1(s\Delta\tau),\ x_2(s\Delta\tau),\ \cdots,\ x_k(s\Delta\tau))\quad (s = 1,\ \cdots,\ N)$. Then, the AR process for $X(s)$ can be written as

$$x_i(s) = \sum_{m=1}^{M}\sum_{j=1}^{k} A_{ij}(m)\ x_j(s-m) + \varepsilon_i(s), \qquad i = 1,\ 2,\ \ldots,\ k, \tag{6.1}$$

where s, $\Delta\tau$ and N denote the time, the sampling interval and the sample number, respectively, $A_{ij}(m)$ is the $(i,\ j)$th element of a coefficient matrix $\boldsymbol{A}(m)$ of $k\times k$ dimension, and the $\varepsilon_i(s)$ are mutually independently and identically distributed random variables. Let $A_{Mij}(m)$ be the component of the matrix $A_{ij}(m)$ with length M, which is determined so as to minimize the expected value of $\varepsilon_i(s)^2$ using (6.1), and let $\boldsymbol{A}_M(m)$ be the matrix with the components $A_{Mij}(m)$. The essential points of system identification are twofold: the appropriate estimation of the coefficient matrix $\boldsymbol{A}_M(m)$ and the determination of the optimal length of M. In the present study, in order to satisfy these requirements, we apply the Yule–Walker scheme (e.g. see Parzen 1974) to the estimation of $\boldsymbol{A}_M(m)$ in combination with Akaike's method (Akaike 1971, 1974) for determining M. The procedure can be summarized in the following five steps [1]–[5].

[1] Remove the averaged value from $x_i(s)$.

[2] Calculate the cross-correlation coefficient

$$C_{ij}(\ell) = \frac{1}{N}\sum_{s=1}^{N-\ell} x_i(s+\ell)\ x_j(s), \qquad \ell = 0,\ 1,\ \ldots,\ L, \tag{6.2}$$

for $i,\ j = 1,\ 2\ \cdots,\ k$. In the right-hand side of (6.2), the denominator is not $N-\ell$ but N to realize better estimation for C_{ij} (Fuller 1976). In the following, $\boldsymbol{C}(\ell)$ represents the $k \times k$ matrix whose $(i,\ j)$th element is $C_{ij}(\ell)$, and the superscripts T and -1 denote transposed and inverse matrices, respectively.

[3] Set $\boldsymbol{A}_0(m) = \boldsymbol{B}_0(m) = \boldsymbol{O}$ (zero matrix) for $m = 1,\ 2,\ \cdots,\ L, \boldsymbol{d}_0 = \boldsymbol{f}_0 = \boldsymbol{C}(0)$, and $\boldsymbol{e}_0 = \boldsymbol{C}(1)$.

[4] Determine $\boldsymbol{A}_M(m)\ (m = 1,\ 2,\ \cdots,\ M)$ and $\boldsymbol{d}_M$ successively for $M = 1, 2, \cdots, L$ using the following set of equations:

$$\left.\begin{aligned} \boldsymbol{d}_M &= \boldsymbol{C}(0) - \sum_{m=1}^{M} \boldsymbol{A}_M(m)[\boldsymbol{C}(m)]^{\mathrm{T}}, \\ \boldsymbol{e}_M &= \boldsymbol{C}(M+1) - \sum_{m=1}^{M} \boldsymbol{A}_M(m)\boldsymbol{C}(M+1-m), \\ \boldsymbol{f}_M &= \boldsymbol{C}(0) - \sum_{m=1}^{M} \boldsymbol{B}_M(m)\boldsymbol{C}(m), \\ \boldsymbol{D}_M &= \boldsymbol{e}_M[\boldsymbol{f}_M]^{-1}, \\ \boldsymbol{E}_M &= [\boldsymbol{e}_M]^{\mathrm{T}}[\boldsymbol{d}_M]^{-1}; \end{aligned}\right\} \tag{6.3}$$

$$\left.\begin{aligned} \boldsymbol{A}_{M+1}(m) &= \boldsymbol{A}_M(m) - \boldsymbol{D}_M\boldsymbol{B}_M(M+1-m) \\ \boldsymbol{B}_{M+1}(m) &= \boldsymbol{B}_M(m) - \boldsymbol{E}_M\boldsymbol{A}_M(M+1-m) \end{aligned}\right\} \text{for } m = 1,\ 2,\ \cdots,\ M, \tag{6.4}$$

$$\left.\begin{aligned} \boldsymbol{A}_{M+1}(m) &= \boldsymbol{D}_M \\ \boldsymbol{B}_{M+1}(m) &= \boldsymbol{E}_M \end{aligned}\right\} \text{for } m = M+1. \tag{6.5}$$

[5] Calculate the following multiple final prediction error (MFPE) when executing step [4]:

$$\mathrm{MFPE}(M) = \left[1 + \frac{Mk+1}{N}\right]^{k} \left[1 - \frac{Mk+1}{N}\right]^{-k} \| \boldsymbol{d}_M \| \tag{6.6}$$

and determine M so as to make MFPE(M) minimum for $M = 0,\ 1,\ \cdots,\ L$. Here $\| \boldsymbol{d}_M \|$ denotes the determinant of the matrix $\boldsymbol{d}_M$ and gives the estimation for covariance of the white noise $\varepsilon_i(s)$.

We have predicted the temperature fluctuations in the wall region for the four key patterns (figure 6) and the Q3-Q2-Q3 pattern (figure 9) by substituting $\boldsymbol{A}_M(m)$ and $\varepsilon_i(s)$, determined by the above AR procedure with the inputs $x_1 = \hat{u}$, $x_2 = \hat{v}$, and the output $x_3 = \hat{t}$, into (6.1). The results are shown in figure 13. In this prediction, we have set $\varepsilon_i(s) = 0$ to compare the predicted results with those obtained by the TRAT. As seen clearly from figure 13, the predictions from the AR model† are in almost perfect agreement with the $\langle t \rangle$-patterns extracted by the TRAT. This fact supports the effectiveness of the AR model in predicting and analysing the turbulent heat transfer associated with coherent structures near the wall.

† In the present AR model, we have used the MFPE function to determine the model order M, which will minimize the final prediction error by keeping the number of parameters as small as possible. The value of MFPE decreases steeply at the initial stage, takes a minimum and increases gradually as the order M increases. The value of M, at which the MFPE becomes minimum, changes with the distance from the wall y, i.e. M ranges from 10 to 15 at a sampling frequency 32 kHz, which corresponds to time in wall units $\tau^+ = 9.2$–13.8. It is interesting that this value happens to accord with the averaging time τ_{av}^+ used in the VITA technique.

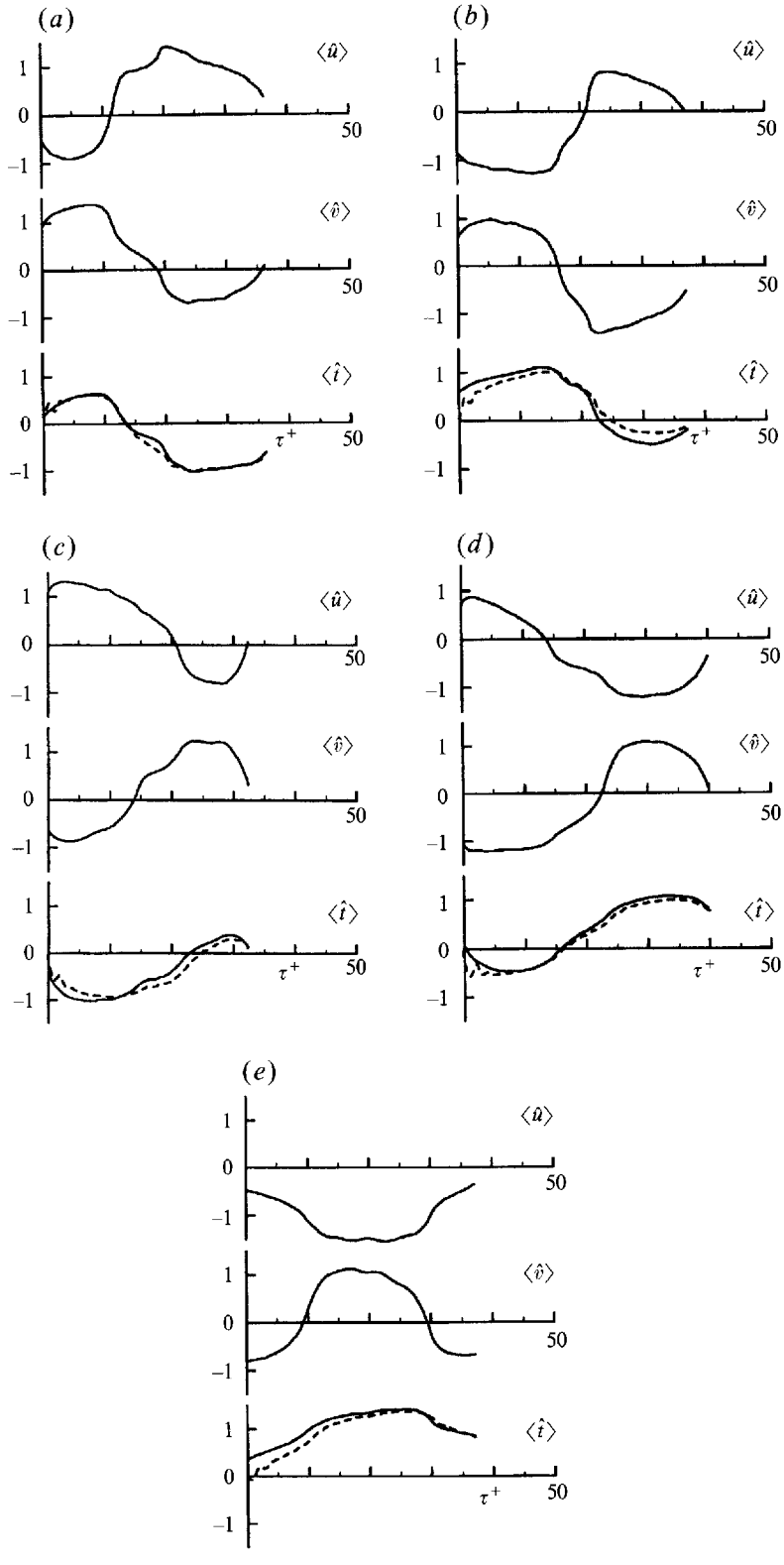

FIGURE 13. Predictions of near-wall temperature fluctuations associated with the key flow patterns using the autoregressive (AR) model: ————, measurements; – – – –, AR model prediction. (*a*) Q2-Q1-Q4; (*b*) Q2-Q3-Q4; (*c*) Q4-Q1-Q2; (*d*) Q4-Q3-Q2; (*e*) Q3-Q2-Q3.

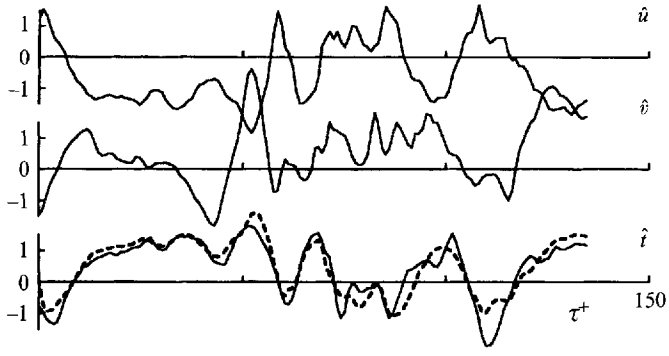

FIGURE 14. Predictions of instantaneous temperature fluctuations near the wall using the autoregressive (AR) model: ———, measurements; – – – –, AR model prediction.

To check the total performance of the present AR model, we have predicted temperature fluctuations at $y^+ = 18.5$ by putting the measured fluctuating velocity components u and v into the algorithm for the AR model prediction. The sample result is shown in figure 14. The predictions trace the instantaneous temperature fluctuations precisely. This means that we can apply the AR model to the prediction of near-wall thermal field which is the key region for effective control of turbulent heat transfer.

In sum, if we input some controlled velocity fluctuations, u and v, into the AR model, we can predict the relevant turbulent heat transfer caused by inputted fluid motions. Thus, the present approach based on the modern control theory for a dynamic system may give a potential tool for establishing a method for controlling turbulence and related transport phenomena.

7. Conclusions

Investigations of the coherent motions and relevant heat transfer in wall turbulence have been performed using the improved trajectory analysis technique (TRAT) and the autoregressive (AR) model predictions. The results can be summarized as follows.

(i) To reveal the detailed characteristics of turbulent heat and momentum transport associated with coherent motions, it is of fundamental importance to clarify the phase relations between the fluctuating components of velocity and temperature. Thus, a detection scheme with phase information is indispensable for this purpose. The present TRAT developed and improved based on the quadrant splitting scheme satisfies this requirement and has the potential for clarifying the essential features of turbulent transport phenomena. (A preliminary version of the TRAT was proposed by Nagano & Hishida (1990). However, the fundamental aspects of the present TRAT are essentially different because of classifying fluid motions into the 36 flow modules of a sequence of three quadrants in the (u, v)-plane and adding the essential improvements to the trajectory analysis technique (for example, elimination of noise-like fluid motions in a trajectory). The bone structure of the TRAT has become firm for the first time in the present study.)

(ii) Since VITA events consist of various fluid motions, each with different phase characteristics, this technique does not allow appropriate classification of the events responsible for heat transfer, even with the addition of the slope criterion to the scheme.

(iii) In wall turbulence, there are four key flow patterns with distinct phase characteristics which play an important role in the dynamics and transport phenomena of turbulence: Q2-Q1-Q4, Q2-Q3-Q4, Q4-Q1-Q2 and Q4-Q3-Q2 patterns.

(iv) The Q3-Q2-Q3 pattern also contributes largely to turbulent heat transfer, which is not a violent event and cannot be detected by the VITA technique. However, this pattern contains strong Q2-motions causing huge heat transfer.

(v) Three significant parts of the ejections extracted by the flow visualization experiment (Bogard & Tiederman 1987) have been specified by the TRAT. Namely, leading edge, middle and trailing edge correspond to the trajectories Q4-Q3-Q2, Q3-Q2-Q3 and Q2-Q3-Q4, respectively, and two of them, Q4-Q3-Q2 and Q2-Q3-Q4, belong to the key patterns extracted by the TRAT. The quantitative relations between each ejection phase and heat transport have been made clear.

(vi) The AR model can predict properly the ensemble-averaged characteristics of turbulent heat transfer associated with coherent structures near the wall.

It is widely accepted that each detection scheme detects mostly the 'events' which it is designed to detect. The TRAT, on the other hand, is designed to evaluate a fluid motion (turbulence structure) rather than only to detect an event. By applying the TRAT to the analysis of wall turbulence, we have found that all patterns with a strong interactive motion between Q2 and Q4 motions can be considered basic and independent, since they show very different phase characteristics from one another as seen in figures 6 and 12. Thus, these key patterns (flow modules) can be used as a guide to probe the structures of wall turbulence. Recently, analysis of three-dimensional structures of turbulence and heat transfer has been started using DNS databases (e.g. Kasagi & Ohtsubo 1993). Our next task may be to determine the three-dimensional characteristics of the key patterns obtained in the present study.

REFERENCES

AKAIKE, H. 1971 Autoregressive model fitting for control. *Ann. Inst. Statist. Maths* **23**, 163–180.

AKAIKE, H. 1974 A new look at the statistical model identification. *IEEE Trans. Automatic Control* **19**, 716–723.

ALFREDSSON, P. H. & JOHANSSON, A. V. 1984 On the detection of turbulence-generating events. *J. Fluid Mech.* **139**, 325–345.

ANTONIA, R. A., RAJAGOPALAN, S., SUBRAMANIAN, C. S. & CHAMBERS, A. J. 1982 Reynolds-number dependence of the structure of a turbulent boundary layer. *J. Fluid Mech.* **121**, 123–140.

BLACKWELDER, R. F. & KAPLAN, R. E. 1976 On the wall structure of the turbulent boundary layer. *J. Fluid Mech.* **76**, 89–112.

BOGARD, D. G. & TIEDERMAN, W. G. 1986 Burst detection with single-point velocity measurements. *J. Fluid Mech.* **162**, 389–413.

BOGARD, D. G. & TIEDERMAN, W. G. 1987 Characteristics of ejections in turbulent channel flow. *J. Fluid Mech.* **179**, 1–19.

BRODKEY, R. S., WALLACE, J. M. & ECKELMANN, H. 1974 Some properties of truncated turbulence signals in bounded shear flows. *J. Fluid Mech.* **63**, 209–224.

CHEN, C.-H. P. & BLACKWELDER, R. F. 1978 Large-scale motion in a turbulent boundary layer: A study using temperature contamination. *J. Fluid Mech.* **89**, 1–31.

FARGE, M. 1992 Wavelet transforms and their applications to turbulence. *Ann. Rev. Fluid Mech.* **24**, 395–457.

FULLER, W. R. 1976 *Introduction to Statistical Time Series.* John Wiley & Sons.

HISHIDA, M. & NAGANO, Y. 1978*a* Structure of turbulent temperature and velocity fluctuations in the thermal entrance region of a pipe. In *Proc. 6th Intl Heat Transfer Conf., Toronto*, vol. 2, pp. 531–536.

HISHIDA, M. & NAGANO, Y. 1978*b* Simultaneous measurements of velocity and temperature in nonisothermal flows. *Trans. ASME* C: *J. Heat Transfer* **100**, 340–345.

HISHIDA, M. & NAGANO, Y. 1979 Structure of turbulent velocity and temperature fluctuations in fully developed pipe flow. *Trans. ASME* C: *J. Heat Transfer* **101**, 15–22.

HISHIDA, M. & NAGANO, Y. 1988*a* Turbulence measurements with symmetrically bent V-shaped hot-wires. Part 1. Principles of operation. *Trans. ASME* I: *J. Fluids Engng* **110**, 264–269.

HISHIDA, M. & NAGANO, Y. 1988*b* Turbulence measurements with symmetrically bent V-shaped hot-wires. Part 2. Measuring velocity components and turbulent shear stresses. *Trans. ASME* I: *J. Fluids Engng* **110**, 270–274.

HISHIDA, M., NAGANO, Y. & TAGAWA, M. 1986 Transport processes of heat and momentum in the wall region of turbulent pipe flow. In *Proc. 8th Intl Heat Transfer Conf., San Francisco*, vol. 3, pp. 925–930. Hemisphere.

HUNT, J. C. R., KEVLAHAN, N. K.-R., VASSILICOS, J. C. & FARGE, M. 1993 Wavelets, fractals and Fourier transforms: detection and analysis of structure. In *Wavelets, Fractals, and Fourier Transforms* (ed. M. Farge, J. C. R. Hunt & J. C. Vassilicos), pp. 1–38. Clarendon.

IRITANI, Y., KASAGI, N. & HIRATA, M. 1985 Heat transfer mechanism and associated turbulence structure in the near-wall region of a turbulent boundary layer. In *Turbulent Shear Flows 4* (ed. L. J. S. Bradbury, F. Durst, B. E. Launder, F. W. Schmidt & J. H. Whitelaw), pp. 223–234. Springer.

JOHANSSON, A. V. & ALFREDSSON, P. H. 1982 On the structure of turbulent channel flow. *J. Fluid Mech.* **122**, 295–314.

JOHANSSON, A. V., ALFREDSSON, P. H. & KIM, J. 1991 Evolution and dynamics of shear-layer structures in near-wall turbulence. *J. Fluid Mech.* **224**, 579–599.

KASAGI, N. 1990 Structural study of near-wall turbulence and its heat transfer mechanism. In *Near-Wall Turbulence* (ed. S. J. Kline & N. H. Afgan), pp. 596–619. Hemisphere.

KASAGI, N. & OHTSUBO, Y. 1993 Direct numerical simulation of low Prandtl number thermal field in a turbulent channel flow. In *Turbulent Shear Flows 8* (ed. F. Durst, R. Friedrich, B. E. Launder, F. W. Schmidt, U. Schumann & J. H. Whitelaw), pp. 97–119. Springer.

KASAGI, N., TOMITA, Y. & KURODA, A. 1992 Direct numerical simulation of passive scalar field in a turbulent channel flow. *Trans. ASME C: J. Heat Transfer* **114**, 598–606.

KIM, J. & MOIN, P. 1989 Transport of passive scalars in a turbulent channel flow. In *Turbulent Shear Flows 6* (ed. J.-C. André, J. Cousteix, F. Durst, B. E. Launder, F. W. Schmidt & J. H. Whitelaw), pp. 85–96. Springer.

KLINE, S. J. 1990 Quasi-coherent structures in the turbulent boundary layer: Part I. Status report on a community-wide summary of the data. In *Near-Wall Turbulence* (ed. S. J. Kline & N. H. Afgan), pp. 200–217. Hemisphere.

LU, S. S. & WILLMARTH, W. W. 1973 Measurements of the structure of the Reynolds stress in a turbulent boundary layer. *J. Fluid Mech.* **60**, 481–511.

LUCHIK, T. S. & TIEDERMAN, W. G. 1987 Timescale and structure of ejections and bursts in turbulent channel flows. *J. Fluid Mech.* **174**, 529–552.

MORRISON, J. F., TSAI, H. M. & BRADSHAW, P. 1989 Conditional-sampling schemes for turbulent flow, based on the variable-interval time averaging (VITA) algorithm. *Exps. Fluids* **7**, 173–189.

NAGANO, Y. & HISHIDA, M. 1985 Production and dissipation of turbulent velocity and temperature fluctuations in fully developed pipe flow. In *Proc. 5th Symp. on Turbulent Shear Flows, Cornell University, Ithaca*, pp. 14.19–14.24.

NAGANO, Y. & HISHIDA, M. 1990 Turbulent heat transfer associated with coherent structures near the wall. In *Near-Wall Turbulence* (ed. S. J. Kline & N. H. Afgan), pp. 568–581. Hemisphere.

NAGANO, Y., SATO, H. & TAGAWA, M. 1995 Structure of heat transfer in the thermal layer growing in a fully developed turbulent flow. In *Turbulent Shear Flows 9* (ed. F. Durst, N. Kasagi, B. E. Launder, F. W. Schmidt, K. Suzuki & J. H. Whitelaw), pp. 343–364. Springer.

NAGANO, Y. & TAGAWA, M. 1988 Statistical characteristics of wall turbulence with a passive scalar. *J. Fluid Mech.* **196**, 157–185.

NAGANO, Y. & TAGAWA, M. 1990 A structural turbulence model for triple products of velocity and scalar. *J. Fluid Mech.* **215**, 639–657.

NAGANO, Y. & TSUJI, T. 1994 Recent developments in hot- and cold-wire techniques for measurements in turbulent shear flows near walls. *Expl Thermal Fluid Sci.* **9**, 94–110.

PARZEN, E. 1974 Some recent advances in time series modeling. *IEEE Trans. Automatic Control* **19**,

723–730.

ROBINSON, S. K. 1991*a* Coherent motions in the turbulent boundary layer. *Ann. Rev. Fluid Mech.* **23**, 601–639.

ROBINSON, S. K. 1991*b* The kinematics of turbulent boundary layer structure. *NASA Tech. Memo.* 103859.

ROBINSON, S. K., KLINE, S. J. & SPALART, P. R. 1990 Quasi-coherent structures in the turbulent boundary layer: Part II. Verification and new information from a numerically simulated flat-plate layer. In *Near-Wall Turbulence* (ed. S. J. Kline & N. H. Afgan), pp. 218–247. Hemisphere.

SPINA, E. F., DONOVAN, J. F. & SMITS, A. J. 1991 On the structure of high-Reynolds-number supersonic turbulent boundary layers. *J. Fluid Mech.* **222**, 293–327.

SUBRAMANIAN, C. S., RAJAGOPALAN, S., ANTONIA, R. A. & CHAMBERS, A. J. 1982 Comparison of conditional sampling and averaging techniques in a turbulent boundary layer. *J. Fluid Mech.* **123**, 335–362.

TAGAWA, M., TSUJI, T. & NAGANO, Y. 1992 Evaluation of X-probe response to wire separation for wall turbulence measurements. *Exps. Fluids* **12**, 413–421.

TSUJI, T., NAGANO, Y. & TAGAWA, M. 1992 Frequency response and instantaneous temperature profile of cold-wire sensors for fluid temperature fluctuation measurements. *Exps. Fluids* **13**, 171–178.

WALLACE, J. M., BRODKEY, R. S. & ECKELMANN, H. 1977 Pattern-recognized structures in bounded turbulent shear flows. *J. Fluid Mech.* **83**, 673–693.

WROBLEWSKI, D. E. & EIBECK, P. A. 1991 A frequency response compensation technique for cold wires and its application to a heat flux probe. *Exp. Thermal Fluid Sci.* **4**, 452–463.